SCIENTIA BRUNEIANA

OFFICIAL JOURNAL OF
THE FACULTY OF SCIENCE
UNIVERSITI BRUNEI DARUSSALAM

ISSN : 1819-9550 (Print), 2519-9498 (Online) - Volume : 17(2), 2018

First Published 2018 by

Faculty of Science,
Universiti Brunei Darussalam
Jalan Tungku Link
Bandar Seri Begawan BE1410
Brunei Darussalam

This book consists of papers prepared by staff of Universiti Brunei Darussalam and other academic institutions, and peer-reviewed by local and international referees.

Cataloguing in Publication Data

Scientia Bruneiana / Chief Editor Lim Lee Hoon

46 p. + iii; 30 cm

ISSN 2519-9498 (Online), ISSN 1819-9550 (Print)

1. Research – Brunei Darussalam. 2. Science – Brunei Darussalam

Q180.B7 B788 2018

Cover photo: Activity of protease extracted from mixed fruits on skimmed milk agar after incubation.
(Courtesy: Yeo Yen Chin, Roemah Goeting, Yabit bin Alas and Pooja Shivanand).

Printed in Brunei Darussalam by
Educational Technology Centre,
Universiti Brunei Darussalam

mk

SCIENTIA BRUNEIANA

A journal of science and science-related matters published twice a year (January-June and July-December) by the Faculty of Science, University Brunei Darussalam. Contributions are welcomed in any area of science, mathematics, medicine or technology. Authors are invited to submit manuscripts to the editor or any other member of the Editorial Board. Further information including instructions for authors can be found in the Notes to Contributors section (the last three pages).

EDITORIAL BOARD

SCIENTIA BRUNEIANA is published by the Faculty of Science,
Universiti Brunei Darussalam, Brunei Darussalam BE 1410

ISSN 2519-9498 (Online), ISSN 1819-9550 (Print)

1. Research – Brunei Darussalam. 2. Science – Brunei Darussalam

Q180.B7 B788 2018

SCIENTIA BRUNEIANA

Publication Ethics Policy

The Editorial Board of *Scientia Bruneiana* is committed to implementing and maintaining the publication standards of a high-quality peer-reviewed scientific journal.

Each manuscript submitted to *Scientia Bruneiana* is examined by a referee with recognised expertise in the manuscript's subject area, and all communications between the referee and the author(s) pass must first through the Editorial Board, so that the identity of the referee remains confidential.

No one will be appointed as the referee of a manuscript if he or she is known to have a potentially compromising relationship with one or more of the authors of the manuscript, as for example in being related through blood or marriage to an author, or in being the research supervisor or research student of an author.

The Editorial Board of *Scientia Bruneiana* makes every effort to ensure that each paper published in the journal is free of plagiarism, redundant or recycled text, and fabricated or misrepresented data. Where possible, plagiarism detection software will be used to check for plagiarised or recycled text.

Provided that a manuscript is free of the ethical lapses described in the previous paragraph, the decision to publish it in *Scientia Bruneiana* is based entirely on its scientific or academic merit, as judged by the referee. The referee's assessment of the merit of the manuscript is final. While a full statement of the reasons behind the referee's decision will be passed on to the author(s), no appeals from the author(s) will be entertained.

Under no circumstances will the referee of a paper published in *Scientia Bruneiana* be credited as one of the authors of the paper, and other papers that have been authored or co-authored by the referee will be admitted to the paper's list of references only after an independent third party with expertise in the area has been consulted to ensure that the citation is of central relevance to the paper.

If a member of the Editorial Board of *Scientia Bruneiana* is listed as an author of a manuscript submitted to *Scientia Bruneiana*, that Board member will play no part whatsoever in the processing of the manuscript.

Where necessary, any corrections or retractions of papers previously published in *Scientia Bruneiana* will be printed in the earliest possible edition of the journal, once the need for a correction or retraction has been drawn to the attention of the Editorial Board.

SCIENTIA BRUNEIANA VOL. 17, NO. 2

2018

Table of Contents **Page Numbers**

From fruit waste to enzymes

Yeo Yen Chin[1], Roemah Goeting[1], Yabit bin Alas[2]and Pooja Shivanand[1]*

[1]Environmental and Life Sciences, Faculty of Science, Universiti Brunei Darussalam, Jalan Tungku Link, Gadong BE 1410, Brunei Darussalam
[2]Language Centre, Universiti Brunei Darussalam, Jalan Tungku Link, Gadong BE 1410, Brunei Darussalam

**corresponding author email: pooja.shivanand@ubd.edu.bn*

Abstract

Domestic and municipal solid wastes pose environmental concerns and health risks, suggesting the importance of reduced waste disposal. Food waste accounts for the highest percentage of solid waste in Brunei. An effective strategy is to convert food waste into beneficial products such as enzymes and biofertilizers. This study reports utilization of inedible fruit peels as substrates for enzyme production. A fermentation medium prepared by adding fruit peels, brown sugar and water was allowed to ferment over a period of time. Total carbohydrate content was found to be highest in the fermented orange sample (37.87 ± 4.7 mg/mL) followed by pineapple and banana samples, 11.98 ± 1.45 mg/mL and 10.60 ± 0.45 mg/mL, respectively. Pineapple sample showed the highest concentration of reducing sugar (11.93 mg/mL at week 2 and 3.31 mg/mL after 3 months). Enzyme assay showed that citrus fruits like oranges, yield high activities of enzymes like protease (0.129 U/mL), α-amylase (7.261 ± 0.83 U/mL) and cellulase (0.514 ± 0.03 U/mL). This fermentation product of kitchen waste is economical as it uses cheap raw materials, free of chemical additives and hence eco-friendly.

Index Terms: food waste management, fruit enzymes, biocleaners, biofertilizer

1. Introduction

Increase in urbanization has led to a rapid increase in Municipal Solid Waste (MSW). Landfills are a common destination for MSW, leading to environmental and health effects.[1] According to the Department of Environment, Parks and Recreation, Brunei, approximately 400-500 tonnes of waste goes to Sungai Paku landfill in Tutong District each day.[2] Food waste accounts for the highest percentage of MSW in Brunei followed by paper and plastic. Solid waste reduction can effectively begin on a domestic scale by managing household and kitchen waste. An economic and eco-friendly strategy is converting food waste into beneficial products. One example is increasing soil fertility by microbial activity on food waste added to soil.[3] Secondly, enzymes can be produced by fermentation of food waste with applications in domestic and waste water treatment.[4] Thirdly, anaerobic digestion is well-known for treating MSW for biogas production[5] consisting of methane (55-65%), carbon dioxide (30-35%) and other trace gases such as hydrogen and nitrogen.[6]

Recently, enzymes production using domestic waste has garnered interest among communities. Enzymes are biological catalysts that facilitate biochemical reactions. Amylases, proteases, lipases, pectinases are widely used in domestic and industrial applications.[7] Crude solution of these hydrolytic enzymes, generally referred to as bioenzymes (or garbage enzymes) can be easily produced in households using vegetable and fruit wastes. The pioneering study in this field is attributed to Rosukon Poompanvong from Thailand, who is known to have developed methodology for production of *garbage enzymes*.[8] United Nations Food and Agriculture Organization recognized her contribution to

organic farming by using fermented organic waste in 2003. In solid-state fermentation, non-soluble solids are used as substrate and source of nutrients for microorganisms.[9,10] Such solid substrates includes fruit peel, agricultural crops, agro-industrial residues and organic waste.[11] In submerged fermentation, a liquid medium is used for homogeneous mixing of nutrients. According to standard protocol, to ten parts of water, one part of brown sugar or molasses and three parts of food waste are added and mixed in an air-tight container. It is then left to ferment for about three months in a cool, dark place.[12] This fermented solution is essentially the crude decoction of hydrolytic enzymes. Among the several uses of bioenzymes recommended by Thirumurugun, some include: i. dish and laundry cleaning, ii. stain and odour removal, iii. fruits and vegetables cleansing, iv. clearing sink and drain blockages (using blended pulp or enzyme sludge), v. natural insect repellent vi. plant fertilizer.[13] Purified enzymes have several applications in industry and agriculture.[14-16] In this study, fruit waste is used as a substrate of fermentation to produce beneficial enzymes. The relationship between total carbohydrate content, reducing sugar, protein content and enzyme production is recorded for use in domestic applications.

2. Materials and Methods

2.1 Sample collection and fermentation

Household fruit waste such as fruit stalks and peels were collected and fermented in suitable bottles for enzyme production. In this study, peels of orange, pineapple, banana and mixed fruit (pomelo, watermelon and melon) were used as substrates. Mixed fruit sample containing a random selection of fruit peels are observed for a comparative analysis of enzyme concentration with respect to individual selected fruits. In case of comparable enzyme activities in both cases, it would be convenient, in a domestic household, to ferment different fruit peels together instead of segregating them. Two additional fermentation media were prepared for the mixed fruits; one with the addition of baker's yeast (*Saccharomyces cerevisiae*) and another with yoghurt (Lactic Acid Bacteria). At the end of the incubation period, the respective solutions were analysed for various parameters. All experiments were conducted in duplicate, and the results are shown as the mean ± 1 standard deviation.

2.2 Estimation of moisture content

Fruit peels were sliced, placed on a glass petri dish, weighed to record the initial mass and oven-dried at 80 ˚C for 24 hours. After 24 hours, the dry fruit peels were weighed. The dried peels were left in the oven for another 1-2 hours and weighed again to ensure a constant weight is reached. Percentage of moisture in the peels was calculated. Moisture content (%) is defined as the quantity of water content found in a solid sample. The formula to calculate moisture content is shown in ***Equation 1***:[17]

$$\text{Moisture content (\%)} = \frac{\text{Initial weight} - \text{Final weight}}{\text{Initial weight}} \text{X } 100 \qquad (1)$$

2.3 Measurement of pH

Aliquots of respective fermentation solutions were taken every two weeks up to three months for measurement of pH. The pH of solutions was measured using a lab pH meter (Thermo Scientific, Orion Star A211). During fermentation, the solutions turn acidic and hence a drop in pH is expected.

2.4 Estimation of total carbohydrate content

Total carbohydrate was tested using a modified protocol.[18] An aliquot of fermented sample solution was mixed with 1 mL of 5 % aqueous phenol, followed by the addition of 5 mL concentrated sulphuric acid. The mixture was allowed to stand for 10 minutes, then mixed using a vortex mixer for 30 sec and incubated in water bath at 25 ˚C for 20 min. Absorbance was measured at 490 nm and the concentration of total carbohydrate was calculated.

2.5 Estimation of reducing sugar using DNS method

Reducing sugar content was analysed using the dinitrosalicylic (DNS) colorimetric method described by Miller.[19] 3 mL of fermented sample was mixed with 3 mL of DNS reagent and heated

in a boiling water bath for 5 min. The tubes were then cooled under running tap water, before measuring the absorbance of each sample at 575 nm. Sugar content was calculated using glucose standard.

2.6 Estimation of total protein content

Protein estimation was done by using the method described by Bradford.[20] Coomassie dye solution was prepared by mixing 10 mg of Coomassie Brilliant Blue G-250, 10 mL of 88 % phosphoric acid, 4.7 mL of absolute alcohol and diluting the mixture with 100 mL of distilled water. 1 mL of fermented sample solution was mixed with 3 mL of Coomassie dye solution. The mixture was incubated in dark for 5 min and absorbance was measured at 595 nm. Protein content was calculated using the standard curve of bovine serum albumin (BSA).

2.7 Qualitative enzyme assay

Protease was screened using casein agar plate. One litre of the media was composed of 28 g skim milk powder, 5 g casein enzymic hydrolysate, 2.5 g yeast extract, 1 g dextrose, 15 g agar powder and a final pH of 7.0 ± 0.2. The mixture was autoclaved at 121 ˚C for 15 minutes and poured into petri dishes. Fermented solution containing a mixture of crude enzymes was streaked on the plate and incubated for 2 to 3 days at 37 ˚C. Zone of clearance on skim milk agar indicates hydrolysis of casein by proteases.

Cellulase was screened using cellulose agar plate. Nutrient agar (NA) was supplemented with 0.2 % Carboxymethylcellulose sodium salt (Sigma-Aldrich 21902), sterilized at 121 ˚C for 15 minutes and poured into agar plates. The fermented solution was then streaked onto the solidified agar plate for 2-3 days at 25 ˚C. The plates were flooded with 0.3 % Congo-red solution for 10 minutes followed by de-staining with 1 M Sodium Chloride solution. The presence of cellulase is indicated by a translucent zone around the colony.[21]

2.8 Quantitative enzyme assay

Protease assay was carried out using L-tyrosine as standard.[22] 2.5 mL of casein-potassium phosphate buffer (0.65 % casein dissolved in 50 mM potassium phosphate buffer, pH 7.5) was mixed with 0.5 mL enzyme solution and incubated for 10 minutes at 37 ˚C. To arrest the reaction, 5 mL of 10 % Trichloroacetic acid was added to the mixture and incubated at room temperature for 30 minutes. The reaction mixture was filtered to remove precipitate and 2 mL of the filtrate was mixed with 5 mL of 500 mM sodium carbonate buffer. Absorbance was measured at 280 nm after incubation for 30 minutes. One unit (U) per mL of enzyme is defined as the amount of enzyme required to convert one micromole of substrate into product per minute under given temperature and pH.[23]

For α-amylase, the enzyme solution (0.5 mL) was incubated at 25 ˚C for 3 minutes, then 0.5 mL of starch-sodium phosphate buffer (1 % starch, w/v dissolved in 0.02 M sodium phosphate buffer, pH 6.9) was added. The reaction mixture was incubated at room temperature for 5 minutes before 1 mL DNS reagent was added to stop the reaction. The terminated reaction mixture was heated in a boiling water bath for 5 minutes and left to cool. This mixture was then diluted with distilled water to 10 mL. Absorbance was measured at 540 nm and the concentration of enzyme was calculated using a glucose standard.

Cellulase activity was measured using DNS method.[24] The substrate, Carboxymethylcellulose (CMC), was mixed with sodium acetate buffer (1 % CMC, w/v 0.1 M sodium acetate buffer, pH 4.8). 0.5 mL of enzyme solution was added to the CMC-buffer mixture and incubated for 1 hour at 40 ˚C. The reaction was arrested by the addition of 1 mL DNS reagent. Absorbance was measured at OD_{540} and values were calculated using glucose standard.

3. Results and Discussion

3.1 Effect of moisture content

The significance of measuring moisture content of food is to determine its freshness, nutritive value and quality. Food possessing high moisture decay rapidly as high moisture provides optimal conditions for mold and microbial growth.[25]

Estimated moisture range in selected fruit peels was approximately 70-95% (as shown in ***Table 1***). The higher the water content present in fruit peel, the greater the rate of deterioration in a given time.

***Table 1*:** Percentage moisture content of selected fruit peel samples.

Code	Sample	Differences in weight (g)		Moisture content (%)
		Initial	Final	
A	Orange	19.48	5.32	72.69
B	Pineapple	36.09	6.97	80.69
C	Banana	9.22	1.59	82.75
D	Pomelo	19.32	4.13	78.62
E	Watermelon	34.15	4.13	87.91
F	Melon	35.51	3.28	90.76

3.2 Effect of pH

Experimental results in ***Figure 1*** show the pH value of the solutions gradually decrease over time, to a range of pH 3.0-4.0. The drop in pH of the fermentation medium is due to the conversion of sugars present in the mixtures to acids, ethanol and carbon dioxide. Hence, reduction in pH is an indicator of completion of fermentation and corresponds to higher levels of volatile acids and enzymes.[25]

3.3 Total carbohydrate content

Figure 2 summarizes the change in total carbohydrates content after fermentation. The fermented orange sample contained of 37.87 ± 4.7 mg/mL of total carbohydrates which is the highest among the fruit peel samples tested. The estimated carbohydrate content for the pineapple and banana samples were 11.98 ± 1.45 mg/mL and 10.60 ± 0.45 mg/mL, respectively. The addition of Baker's yeast (4.30 ± 0.48 mg/mL) or yoghurt (8.80 ± 1.48 mg/mL) into the mixed fruits sample causes a rapid reduction of total carbohydrate content compared to the mixed fruits sample alone (13.10 ± 0.78 mg/mL). During the first two weeks of fermentation, the initial carbohydrate concentrations for all fruit samples were higher. Existing microbes in various fruit peels grow aerobically in the culture solution for the conversion of these carbohydrates into soluble sugars and other metabolites. Carbohydrates present in the fermented solution may be a mixture of soluble (glucose, fructose and sucrose) and insoluble carbohydrates (cellulose and hemicellulose) broken down by a consortium of microorganisms present in the fruit peel. The presence of carbohydrates at the end of the fermentation period are remains of any unfermented sugars.

Orange peels, which were the only citrus fruit peels used in this study, contain a terpenoid chemical compound called D-limonene, which is an inhibitor of yeast fermentation. High D-limonene content in citrus fruit waste can inhibit microbial growth.[26] Limonene is the major constituent of citrus fruits' essential oil that are reported to have anti-bacterial and anti-inflammatory properties.[27] This further explains the high concentration of carbohydrates measured in the orange peel sample. Another possible reason for the high carbohydrate concentration is the presence of glucose, fructose, galactose, arabinose, xylose and galacturonic acid in the fermentation medium which could have been produced during enzymatic hydrolysis of orange peels.[28] Fermented solutions containing yeast have lower carbohydrate concentration as yeast contains enzymes that catalyse the breakdown of glucose to ethanol and carbon dioxide. The microbial diversity in the fruit peels accompanied with the addition of yeast further contributes to the utilization of carbohydrates for growth and production of useful metabolites.

3.4 Reducing sugar content

Figure 3 shows the reducing sugar content at two and three months of fermentation. The highest concentration of reducing sugar was 11.93 mg/mL (at week 2) and 3.31 mg/mL (at 3 months) for the pineapple sample. In contrast, banana sample had the lowest concentration among other samples (without addition of yeast or yoghurt), with 5.41 mg/mL and 2.17 mg/mL of reducing sugar at week two and at three months, respectively. It is estimated that fermentation caused an overall 60-80% reduction in reducing sugar content during the ten-week period.

Reducing sugars have reactive aldehyde or ketone groups. Glucose, fructose and sucrose are known to be the main carbohydrates present in fruit peels. Sucrose is a non-reducing sugar. The percentage of reducing sugar is about 30 % of total carbohydrate content for most fruit peels. However, orange peels only contain 6 % reducing sugar of total carbohydrates. During enzymatic hydrolysis of orange peels, the desired reaction is the release of monosaccharides from cellulose and hemicellulose.[25] The accumulation of limonene disrupts microbial growth and hence the release of sugar monomers into the fermented solution could be reduced. It was reported that inhibition occurs even at very low limonene concentration resulting in complete failure of fermentation at higher concentrations.[25]

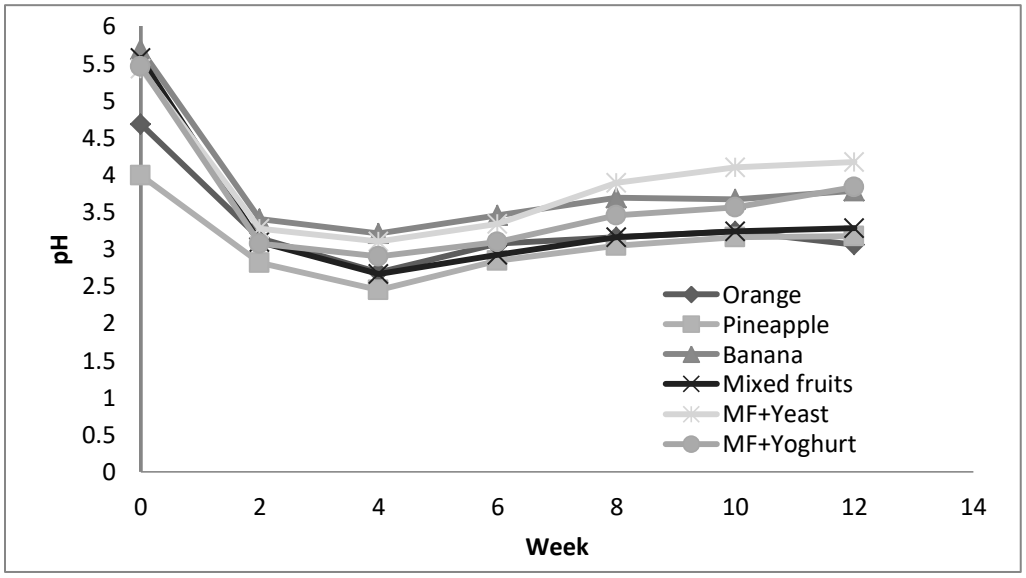

Figure 1. pH recorded for different fermented solutions from week 0 to 12.

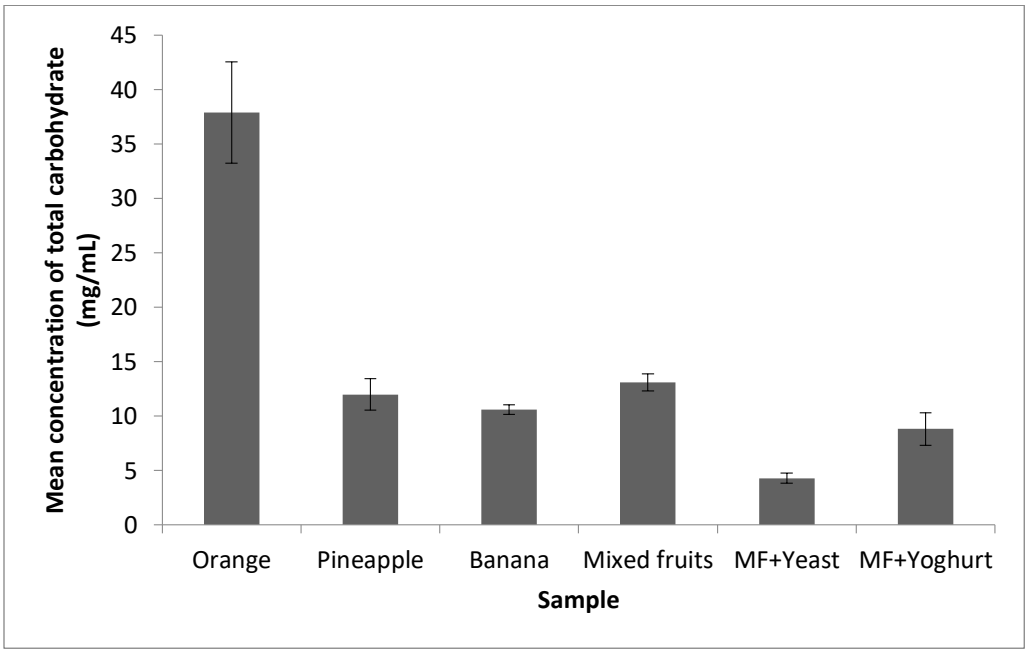

Figure 2. Total carbohydrates concentration at OD_{490} after fruit peels were fermented for three months.

3.5 Total protein content

From ***Figure 4***, the concentration of protein in all fruit waste samples were observed to be low, ranging from 0.176 mg/mL for the mixed fruit sample supplemented with yoghurt, to 0.253 mg/mL for banana peel (two week fermentation medium). After three months of fermentation, the amount of protein is the lowest in the growth medium containing mixed fruits with yoghurt (0.163 mg/mL) and the highest in control mixed fruits (0.285 mg/mL). There is no major decrement in protein concentration from the initial fermentation medium to that after a period of three months. An exception is the mixed fruits fermentation medium control which showed increased protein content. This may be due to different amounts of protein content from a mixture of fruit wastes being released into the fermentation medium which remain underutilized by microbes. Fruit peels with high protein concentration could serve as a possible alternative substrate for cultivation of fungi.[28] Protein is an essential nutrient required for microbial growth and production of enzymes, which might be the reason for the decrease in protein content in the samples.[28,29]

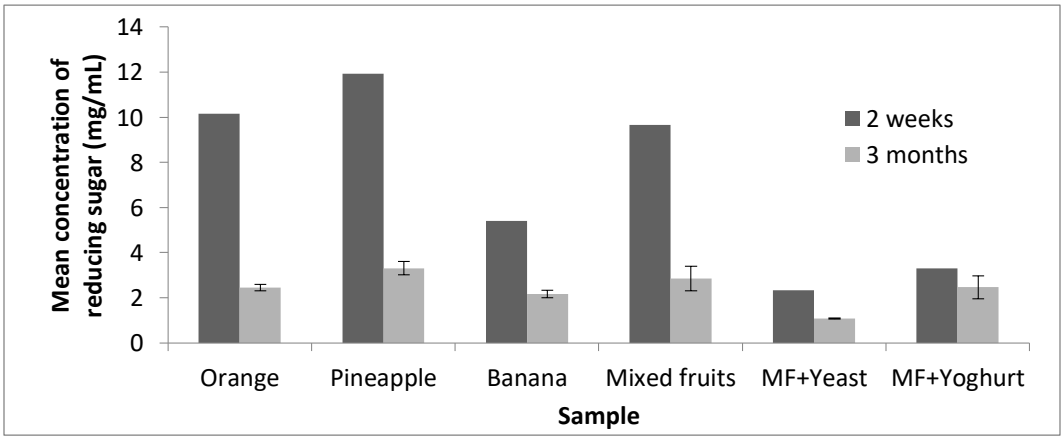

Figure 3. Reducing sugar content at OD_{575} for fruit peels fermented for two weeks and three months.

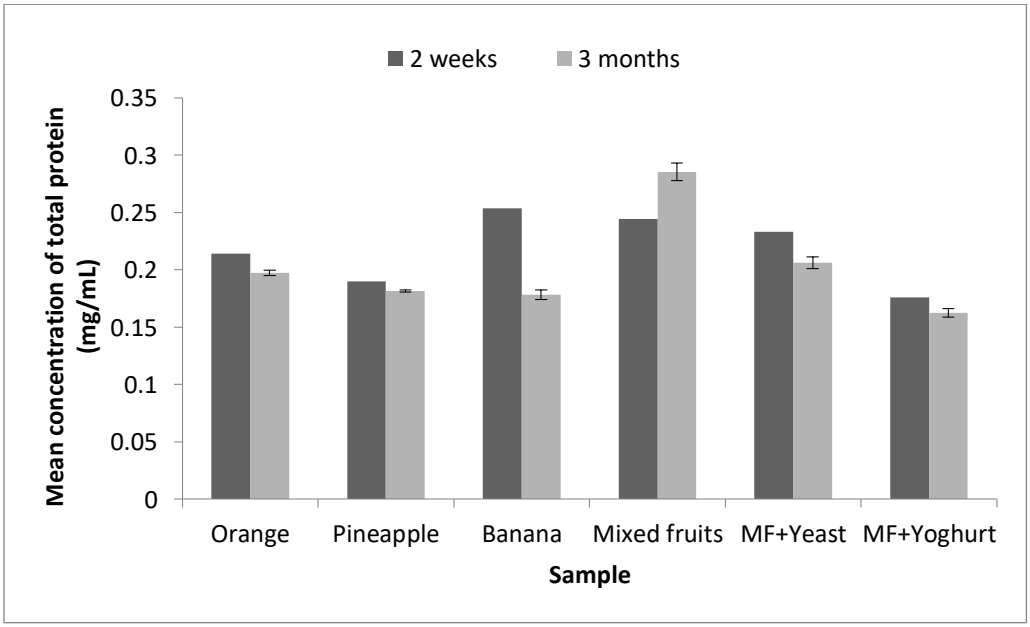

Figure 4. Total protein content at OD_{595} for various fruit peels fermented for two weeks and three months.

3.6 Screening of protease

Figure 5 shows protease activity on skimmed milk agar after incubation at 37 ˚C. The release of protease was observed on each agar plate after three days of incubation. From the zone of clearance observed, all samples contained protease enzymes. Fermented orange solution had the highest protease activity because white-coloured skimmed milk agar turned translucent which signifies complete utilization of the protein by protease-producing microbes. The addition of yoghurt into the fermentation medium introduced probiotic bacteria which, together with the existing microbes in the fruit peels, lead to greater secretion of protease enzymes. The protease activity of fermented samples is shown in ***Figure 6***. Protease concentration was highest in the orange peels sample (0.129 U/mL) and lowest in the mixed fruit with yeast sample (0.041 U/mL). Other fermented samples had a range of protease produced in the solution with 0.046 U/mL for pineapple peels, 0.054 U/mL for banana, 0.081 U/mL for mixed fruits (control) and 0.073 U/mL for mixed fruits supplemented with yoghurt.

Figure 5. Qualitative screening of protease from the mixed fruits with yoghurt sample, after incubating at 37 ˚C on skimmed milk agar plate. Zone of clearance indicates protease activity.

The relationship between microbial growth and protease production has been previously reported[22] where protease secretion by microorganism can be partially inducible in nature to produce extracellular proteases under most growth conditions. However, proteolytic activity tends to be relatively low in yeast. A possible reason for low proteolytic activity in mixed fruits with yeast could be due to ethanol toxicity in yeast from the accumulation of ethanol as the by-product during fermentation, which causes the inactivation of yeast enzymes.

3.7 α-amylase content

The activity of α-amylase was determined by analysing the hydrolysis of soluble starch spectrophotometrically. ***Figure 7*** shows the α-amylase enzymatic activities of the six fermented solutions. As seen from the figure, fermented orange peel sample was found to contain the highest α-amylase concentration with 7.261 ± 0.83 U/mL which was approximately 3 to 4 times higher compared to the other samples. In contrast, the mixed fruit with yeast sample had the lowest α-amylase activity (0.615 ± 0.07 U/mL).

Orange peel offers a rich source of carbon for fermentation as it is rich in fermentable sugars (glucose, fructose and sucrose).[23] Hence it contains sufficient carbon for microbial growth and enzyme production. As reported in literature,[30] extra-cellular α-amylase production is affected by pH. The pH of the fermented orange sample in the present study was pH 3 (***Figure 1***). Starch used as substrate in enzyme analysis, acts as an inexhaustible carbon source for the synthesis of α-amylase in comparison with other carbon sources due to its enzyme stabilization ability.[31,32]

A low α-amylase activity in yeast was observed in this study (***Figure 7***). Little research has been done on α-amylase production in yeast, *Saccharomyces cerevisiae*. One study[33] reports that yeast exhibit no effect on α-amylase production. Most studies reported that the production of fungal amylase is limited to a number of species, particularly *Aspergillus* and *Penicillium* species.[34] *Aspergillus oryzae* has received much attention in research interest due to its capability of producing high amounts of

valuable proteins and industrial enzymes such as α-amylase.[35]

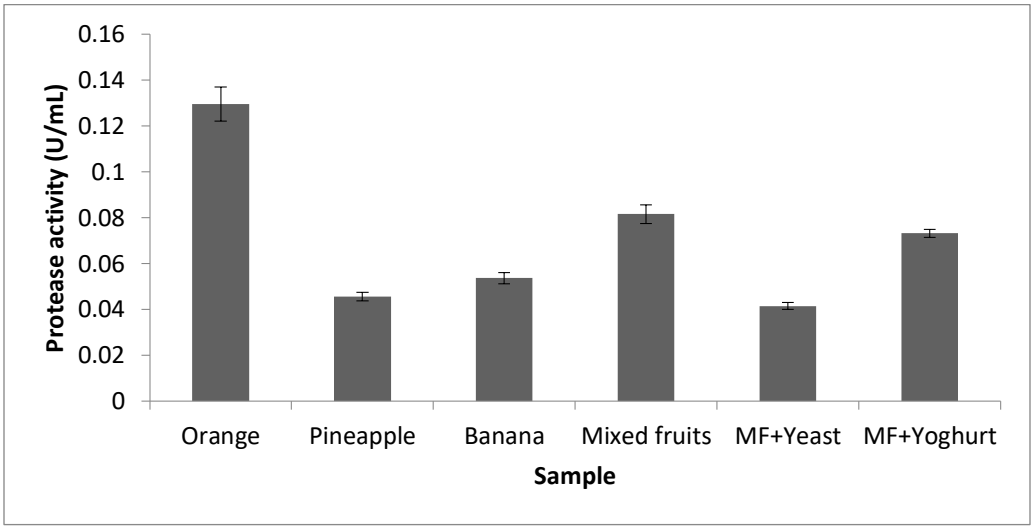

Figure 6. Protease activity for different fermented solution after three months of fermentation.

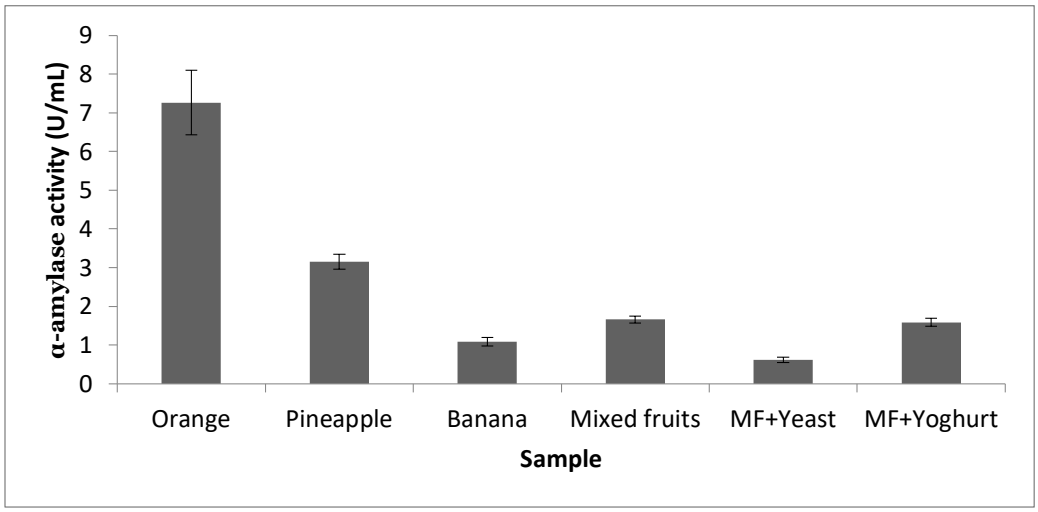

Figure 7. α-amylase activity for different fruit peels samples after three months of fermentation.

3.8 Cellulase assay

Qualitative screening of cellulase activity was carried out on nutrient agar plate containing carboxymethylcellulose (CMC) as substrate. Screening for cellulase was done by staining with congo-red solution for clear observance of enzyme activity. A faint zone of clearance surrounding the culture growth indicates the presence of cellulase enzyme. The appearance of the halo zone around the bacterial or fungal colony provides strong evidence that microbes produced cellulase in order to degrade CMC which is used as the sole source of carbon in the media. After screening for the cellulolytic potential of enzymes produced during fermentation of fruit wastes, spectrophotometric analysis was carried out to quantify cellulase activity. Aliquots of crude enzyme were obtained from each sample solution to analyse the cellulase concentration, as described in the protocol. According to ***Figure 8***, the orange peels showed the highest cellulase activity, reaching 0.514 ± 0.03 U/mL, after three months of fermentation. The three fruit peels namely

pineapple, banana and mixed fruits with yeast showed similar enzymatic activities of 0.123 ± 0.01 U/mL, 0.134 ± 0.00 U/mL and 0.101 ± 0.01 U/mL, respectively. Enzyme activities depend on the release of acidic by-products in the fermentation media.[36] Another possible reason for the decrease in cellulase activity after three months of fermentation is the loss of moisture content during fermentation and inactivation by reduction in pH.[37] The optimum pH of cellulase is between pH 5 to 6.[38]

The fermented solution serves as a crude mixture of hydrolytic enzymes like amylases and proteases. The solution can be filtered and stored in bottles for domestic use. The enzyme filtrate can be used in domestic cleaning and stain removal applications. By optimising their use in domestic cleaning one can reduce the use of commercial chemical detergents. The residue obtained after filtering the solution can either be used for the next batch of fermentation or used as fertilizer.

4. Conclusion

Domestic wastes, mainly food arise in large quantities due to growing demands of increasing population, thereby posing challenges of waste disposal. Hence it is imperative to devise strategies for reduced waste by converting them into useful products like enzymes and fertilizers. Moreover, over the years, there is a roused public concern regarding the potential ecological disadvantages of using synthetic cleaning agents which release toxic chemicals that disrupt environmental pH balance. Fermentation of certain food wastes into enzymes can serve as useful cleaning products due to their specificity, high biodegradability and low toxicity.

The present investigation attempts such an economical and eco-friendly alternative to managing kitchen waste like inedible parts of fruits by converting them into beneficial enzymes. Orange peels are seen to be a promising source of enzymes among the fruit wastes investigated. The crude enzyme solutions were seen to be useful in domestic cleaning and stain removal. Further investigation and repeatability of the established protocols is needed to yield reproducible results. Further trials are needed to scale up processes by optimizing fermentation parameters and developing suitable formulations with enhanced appeal and shelf-life of enzyme based cleaning products.

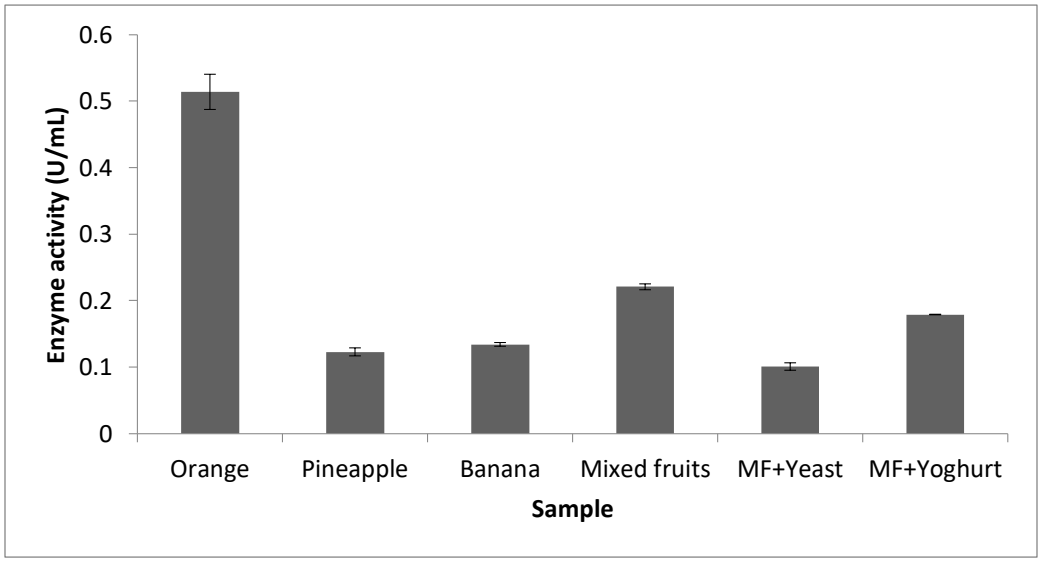

Figure 8. Cellulase activity for various fruit peels samples after three months of fermentation.

References

[1] M. Vrijheid, "Health Effects of Residence Near Hazardous Waste Landfill Sites : A Review of Epidemiologic Literature Epidemiologic Studies on Health Effects of Landfill Sites," *Environ. Health Perspect.*, **2000**, vol. 108, no. March, pp. 101–112.

[2] "Env JAPEM."

[3] M. Sharholy, K. Ahmad, G. Mahmood and R. C. Trivedi, "Municipal solid waste management in Indian cities - A review," *Waste Manag.*, **2008**, vol. 28, no. 2, pp. 459–467.

[4] S. Bharathiraja, J. Suriya, M. Krishnan, P. Manivasagan and S. K. Kim, "Production of Enzymes From Agricultural Wastes and Their Potential Industrial Applications," *Adv. Food Nutr. Res.*, **2017**, vol. 80, pp. 125–148.

[5] S. Jain, I. T. Wolf and T. Y. Wah, "Anaerobic digestion of food waste using artificially cultured and natural anaerobes under Mesophilic conditions," *J. Mater. Environ. Sci.*, **2014**, vol. 5, no. 6, pp. 1709–1714.

[6] A. Chapman-Smith and J. E. Cronan, "The enzymatic biotinylation of proteins: A post-translational modification of exceptional specificity," *Trends Biochem. Sci.*, **1999**, vol. 24, no. 9, pp. 359–363.

[7] S. K. Panda, S. S. Mishra, E. Kayitesi and R. C. Ray, "Microbial-processing of fruit and vegetable wastes for production of vital enzymes and organic acids: Biotechnology and scopes," *Environ. Res.*, **2016**, vol. 146, pp. 161–172.

[8] L. I. T. Lou, "The Material Culture of Green Living in Hong Kong," *Anthropol. Now*, **2017**, vol. 9, no. 1, pp. 70–79.

[9] S. R. Couto and M. Á. Sanromán, "Application of solid-state fermentation to food industry-A review," *J. Food Eng.*, **2006**, vol. 76, no. 3, pp. 291–302.

[10] A. Pandey, "Solid-state fermentation," *Biochem. Eng. J.*, **2003**, vol. 13, no. 2–3, pp. 81–84.

[11] A. Pandey, C. R. Soccol and D. Mitchell, "New developments in solid state fermentation: I-bioprocesses and products," *Process Biochem.*, **2000**, vol. 35, no. 10, pp. 1153–1169.

[12] R. Khazanchi, A. Srivastava and M. Joshi, "Bio-Cleanser : Preparation and Analysis," pp. 1–6.

[13] P. Thirumurugan, "Production and Analysis of Enzyme Bio-Cleaners from Fruit and Vegetable Wastes by Using Yeast and Bacteria Tamil Nadu State Council for Higher Education (TANSCHE)," **2016**.

[14] A. Pandey, C. R. Soccol, P. Nigam and V. T. Soccol, "Biotechnological potential of agro-industrial residues. I: Sugarcane bagasse," *Bioresour. Technol.*, **2000**, vol. 74, pp. 69–80.

[15] S. Sivaramakrishnan *et al.*, "alpha-amylases from microbial sources - An overview on recent developments," *Food Technol. Biotechnol.*, **2006**, vol. 44, no. 2, pp. 173–184.

[16] P. S. Nigam, "Microbial enzymes with special characteristics for biotechnological applications," *Biomolecules*, **2013**, vol. 3, no. 3, pp. 597–611.

[17] P. Ellaiah, K. Adinarayana, Y. Bhavani, P. Padmaja and B. Srinivasulu, "Optimization of process parameters for glucoamylase production under solid state fermentation by a newly isolated Aspergillus species," *Process Biochem.*, **2002**, vol. 38, no. 4, pp. 615–620.

[18] M. Dubois, K. A. Gilles, J. K. Hamilton, P. A. Rebers and F. Smith, "Colorimetric Method for Determination of Sugars and Related Substances," *Anal. Chem.*, **1956**, vol. 28, no. 3, pp. 350–356.

[19] G. L. Miller, "Use of Dinitrosalicylic Acid Reagent for Determination of Reducing Sugar," *Anal. Chem.*, **1959**, vol. 31, no. 3, pp. 426–428.

[20] M. M. Bradford, "A rapid and sensitive method for the quantitation of microgram quantities of protein utilizing the principle of protein-dye binding," *Anal. Biochem.*, **1976**, vol. 72, no. 1–2, pp. 248–254.

[21] A. Sazci, K. Erenler and A. Radford, "Detection of cellulolytic fungi by using Congo red as an indicator: a comparative study with the dinitrosalicyclic acid reagent method," *J. Appl. Bacteriol.*, **1986**, vol. 61, no. 6, pp. 559–562.

[22] P. Shivanand and G. Jayaraman, "Production of extracellular protease from halotolerant bacterium, Bacillus aquimaris strain VITP4 isolated from Kumta coast," *Process Biochem.*, **2009**, vol. 44, no. 10, pp. 1088–1094.

[23] S. Djekrif-Dakhmouche, Z. Gheribi-Aoulmi, Z. Meraihi and L. Bennamoun, "Application of a statistical design to the optimization of culture medium for α-amylase production by Aspergillus niger ATCC 16404 grown on orange waste powder," *J. Food Eng.*, **2006**, vol. 73, no. 2, pp. 190–197.

[24] C. Florencio, S. Couri and C. S. Farinas, "Correlation between agar plate screening and solid-state fermentation for the prediction of cellulase production by trichoderma strains," *Enzyme Res.*, **2012**, no. November, Article ID 793708.

[25] Z. G. Eman, "Bioconversion of orange peels for ethanol production using Bacillus subtilis and Pseudomonas aeruginosa," *African J. Microbiol. Res.*, **2013**, vol. 7, no. 14, pp. 1266–1277.

[26] K. Grohmann, R. G. Cameron and B. S. Buslig, "Fractionation and pretreatment of organge peel by dilute acid hydrolysis," *Bioresour. Technol.*, **1995**, vol. 8524, no. 95, pp. 129–141.

[27] "zukerman1951.pdf." .

[28] J. P. Essien, E. J. Akpan and E. P. Essien, "Studies on mould growth and biomass production using waste banana peel," *Bioresour. Technol.*, **2005**, vol. 96, no. 13, pp. 1451–1456.

[29] S. Vaitheki and B. Deepa, "A Comparative Study on the Production of Bioethanol from Individual and Mixed Fruit Wastes," *Imp. J. Interdiscip. Res.*, **2016**, vol. 2, no. 5, pp. 2454–1362.

[30] B. K. Soni, C. Kapp, G. Goma and P. Soucaille, "Solvent production from starch: effect of pH on α-amylase and glucoamylase localization and synthesis in synthetic medium," *Appl. Microbiol. Biotechnol.*, **1992**, vol. 37, no. 5, pp. 539–543.

[31] M. A. Mctique, C. T. Kelly, W. M Fogarty and E. M. Doyle, "Production studies on the alkaline amylases of three alkalophilic *Bacillus spp*." *Biotechnology Letters*, **1994**, *16*(6), 569-574.

[32] G. Aguilar, J. Morlon-Guyot, B. Trejo-Aguilar and J. P. Guyot, "Purification and characterization of an extracellular α-amylase produced by Lactobacillus manihotivorans LMG 18010(T), an amylolytic lactic acid bacterium," *Enzyme Microb. Technol.*, **2000**, vol. 27, no. 6, pp. 406–413.

[33] M. S. Tanyildizi, D. Özer and M. Elibol, "Optimization of α-amylase production by Bacillus sp. using response surface methodology," *Process Biochem.*, **2005**, vol. 40, no. 7, pp. 2291–2296.

[34] K. Kathiresan and S. Manivannan, "a-Amylase production by Penicillium fellutanum isolated from mangrove rhizosphere soil," *African J. Biotechnol.*, **2006**, vol. 5, no. May, pp. 829–832.

[35] B. Jin, H. J. Van Leeuwen, B. Patel and Q. Yu, "Utilisation of starch processing wastewater for production of microbial biomass protein and fungal α-amylase by Aspergillus oryzae," *Bioresour. Technol.*, **1998**, vol. 66, no. 3, pp. 201–206.

[36] S. S. Dhillon, R. K. Gill, S. S. Gill and M. Singh, "Studies on the utilization of citrus peel for pectinase production using fungus Aspergillus niger," *Int. J. Environ. Stud.*, **2004**, vol. 61, no. 2, pp. 199–210.

[37] I. R. Melo, M. F. Pimentel, C. E. Lopes and G. M. T. Calazans, "Application of fractional factorial design to levan production by Zymomonas mobilis," *Brazilian J. Microbiol.*, **2007**, vol. 38, no. 1, pp. 45–51.

[38] P. F. Omojasola, O. P. Jilani and S. A. Ibiyemi, "Cellulase production by some fungi cultured on pineapple waste," *Nat. Sci.*, **2008**, vol. 6, no. 2, pp. 64–79.

Phytochemical characterization of chloroform seed extract from *Schinus molle* collected in the Kingdom of Lesotho

*Manoharan Karuppiah Pillai[1], Kemelo Sanett Matela[1], Mosotho Joseph George[1] and David James Young[2,3,4]**

[1]Faculty of Science and Technology, Department of Chemistry and Chemical Technology, National University of Lesotho, Roma Campus, P. O. Roma 180, Kingdom of Lesotho, Southern Africa
[2]Faculty of Science, Universiti Brunei Darussalam, Jalan Tungku Link, Gadong BE 1410, Brunei Darussalam
[3]School of Science, Monash University Malaysia, 47500 Bandar Sunway, Selangor D.E, Malaysia
[4]College of Engineering, Information Technology and Environment, Charles Darwin University, Darwin, NT 0909, Australia

**corresponding author email: david.young@cdu.edu.au*

Abstract

Chloroform seed extract from *Schinus molle* was analyzed for its phytochemical compositions by GC-MS. A total of 38 compounds were identified. *S. molle* has therapeutic applications in traditional medicine. Essential oils obtained from various parts of this plant are reported to have promising biological and pharmacological activity.

Index Terms: Schinus molle, Anarcardiaceae, chloroform seed extract, GC-MS analysis, phytochemical compositions

1. Introduction

The species *Schinus molle* L. belongs to the Anarcardiaceae family[1-3] and has therapeutic applications in traditional medicine.[4] *S. molle* is native to South and Central America and has been cultivated in Southern African countries. *S. molle* grows to 7-10 m height. The reddish pink fruits (seeds) are edible and taste like pepper (*Piper nigrum*).[3] *S. molle* has antibacterial, analgesic, cytotoxic, anti-inflammatory, antifungal, antiseptic, insecticidal and antioxidant activities.[4-12] The phytochemical compositions of essential oils and extracts obtained from various parts of *S. molle* have previously been reported.[2,10-14] However, the chemical compositions of chloroform seed extract from *S. molle* has not been reported previously, particularly in plants gathered from the Kingdom of Lesotho. The aim of the present study is to determine the phytochemical compositions of chloroform seed extract from *S. molle* collected in the Kingdom of Lesotho by GC-MS analysis. The results thus obtained are communicated in this article.

2. Experimental Method

2.1 Plant materials

Seeds of *S. molle* (115.126g) were collected in August 2017 from Botanical Garden of Roma Campus, National University of Lesotho. The plant material was identified by Mr. Moretloa Polaki, Lecturer, Department of Biology, Faculty of Science and Technology, National University of Lesotho. A voucher specimen (NUL/KM/SM-SEED) is kept at Organic Chemistry Laboratory, Department of Chemistry and Chemical Technology, Faculty of Science and Technology, National University of Lesotho.

2.2 Processing plant materials

The air-dried seeds of *S. molle* were ground into powder using a commercial blender (Waring Blender, Blender 80119, Model HGB2WT93, 240V AC, 50-80 Hz, 3.6 AMPs, Laboratory and Analytical Supplies).

2.3 Preparation of chloroform seed extract

The powdered seeds of *S. molle* was extracted first with chloroform at room temperature and then at reflux condition for 5 hours. The combined extracts were filtered over Whatman No.1 filter paper and 12.91 g of chloroform seed extract was obtained after removal of solvent.

2.4 Analysis of essential oils

GC-MS analysis of the chloroform seed extract was carried out on GC-2010 (Shimadzu, Kyoto, Japan) equipped with a MS-QP2010 mass spectrometer and a Restek Rtx-5ms (5% phenyl-95% dimethylpolysiloxane) capillary column with the dimensions 30 m × 0.25 mm × 0.25 µm. The injection port temperature was set at 200 °C with a split ratio of 1:50. The optimized oven temperature programmer began at 50 °C held for 4 minutes, ramped to 250 °C at a rate of 10 °C/minutes and held for 6 minutes resulting in a total of 30 min. 1.0 µL dilute aliquot was injected in split less mode. Helium (UHP Helium, Afrox, South Africa) was used as carrier gas and was pumped through the column at a constant flow rate of 1 mL/minute. The MS transfer line temperature was set at 250 °C, ion source temperatures was 200 °C, with a scanning mode mass range of 50 – 500 *amu* and the time window was between 4 and 28 min. The acquisition was carried out relative to the tune file that was generated prior to the analysis.

2.5 Identification of chemical compositions

The chemical compositions in the chloroform seed extract were identified by comparison of their MS spectra with NIST/EPA/NIH/NIST08 library data. The relative quantities of the individual compounds in the chloroform seed extract were calculated based on GC peak areas without using correction factors.

3. Results and Discussion

The phytochemical composition of chloroform seed extract from *S. molle* was determined by GC-MS. A total of 38 compounds were identified and are listed in the order of their elution along with the relative percentage and retention time (***Table1***). The chromatogram of the seed extract also is given in ***Figure 1***.

The phytochemical compositions of essential oils of *S. molle* from ripe berries collected in Tunisia,[11] leaves collected in Algeria,[13] fruits and leaves collected in Argentina,[2] fruits, leaves and stems collected in Tunisia,[10] and wood branch collected in Egypt[12] have previously been reported. Recently, the phytochemical compositions of essential oil of *S. molle* from leaves collected in the city of Botucatu, Brazil has been reported.[15] α-Pinene, β-pinene, myrcene, sabinene and epi-α-cadinol have been identified as major compounds in this essential oil.[15] Similarly, the phytochemical compositions of essential oil of *S. molle* from fresh leaves collected in the city of Uruguaiana, Brazil has also been reported. *α*-Pinene, sabinene, bicyclogermacrene and limonene have been identified as major compounds.[16] Garzoli, et al obtained petroleum ether, diethyl ether and acetone extracts from leaves of *S. molle* by sequential extraction.[17] A total of twenty-five compounds have been identified from these three extracts by GC-MS analysis.[17] Elemol has been identified as the most abundant compound followed by bicyclogermacrene, γ-eudesmol, α-eudesmol, β-eudesmol and isocalamendiol.[17] Sesquiterpene and monoterpene hydrocarbons have been identified as the major components in the petroleum ether and diethyl ether extracts while the acetone extracts showed different compositions.[17] Additionally, fatty acid compositions of hexane seed oil extract[3] and variations in total lipids and fatty acids compositions of mature, intermediately mature and immature fruits of *S. molle* have also been reported previously.[14] To the best of our knowledge, the chemical compositions of chloroform seed extract has not been reported previously. Our study indicated that the chemical compositions of this chloroform seed extract is

significantly different from that of essential oils and fatty acids reported in literature.[2,10-17] The essential oils from leaves and fruits of *S. molle* are reported to have significant antimicrobial activities against *Proteus mirabilis,*[1] *E. coli,*[1,2,13,] *S. aureus,*[1,2,13] *P. aeruginosa,*[1,2] *K. pneumonia,*[1] *C. albicans*[1,2,13] and *P. brasiliensis,*[15] and antioxidant activity in DPPH radical scavenging assay.[4,10-12] Recently, the acaricidal effect of the essential oil of *S. molle* on engorged adult females and larval stages of *Rhipicephalus sanguineus* has been evaluated.[18] At a concentration of 2%, the essential oil caused 99.3% of larval mortality.[18] The essential oil also caused inhibition of egg hatching, ovipositional and reproductive efficiency in adult *R. sanguineus* at concentrations of 4 to 20%.[18]

Table 1. Phytochemical compositions of chloroform seed extract from *S. molle*.

Peak No.	Rt. (min)	Peak Area (%)	Identification of Compounds
1	8.800	1.03	7-Methyl-3-methylene-1,6-octadiene
2	9.500	1.04	1-Methyl-2-iso-propylbenzene
3	9.603	5.34	1,5-Dimethyl-1,5-cyclooctadiene
4	10.900	0.64	5,8,10-Undecatrien-3-ol
5	11.247	0.47	Methyl octanoate
6	11.849	0.52	2,6-Dimethyl-1,5,7-octatrien-3-ol
7	12.655	0.53	4-Methylene-1-(1-methylethyl)-acetate-bicyclohexan-3-ol
8	14.449	1.36	5-Hydroxymethyl spiroheptan-5-ol
9	14.775	1.74	1,5,5,6-Tetramethyl-octahydro-1-oxa-cyclopropainden-6-one
10	14.906	0.48	3-Tetradecyn-1-ol
11	15.820	3.08	1,11-Hexadecadiyne
12	16.253	0.90	1,5-Dimethyl-1,4-hexadienyl-1-methyl-1-cyclohexene
13	16.607	2.04	1-Methyl-5-methylene-8-isopropyl-1,6-cyclodecadiene
14	16.781	1.37	1,1,7-Trimethyl-4-methylenedecahydrocyclopropaazulene
15	17.085	3.43	3,3,6,6,9,9-Hexamethyltetracyclononane
16	17.374	1.13	3,7-Dimethyl-2,6-octadienyl butanoate
17	17.721	0.56	Decahydro-1,1,4,7-tetramethylcyclopropeazulen-4-ol
18	17.854	1.66	10,12-Pentacosadiynoic acid
19	17.929	1.90	5-Oxatricyclododecane
20	18.164	1.07	1-Methyl-4-(2-methyloxiranyl)-7-oxabicycloheptane
21	18.231	1.14	4-Cyclopropyl-7-bicycloheptanyl methanol
22	18.389	0.72	Octahydro-1,4,9,9-tetramethyl-7-methanoazulene
23	18.463	1.81	2-Methyl-5-(1-adamantyl)pentan-2-ol
24	18.779	15.33	Decahydrotrimethyl-8-methylene-2-naphthalenemethanol
25	19.181	1.71	1,8-Cyclopentadecadiyne
26	19.269	6.00	(1-Allylcyclopropyl)methanol
27	19.358	3.48	1-Methyl-4-(2-methyloxiranyl)-7-oxabicycloheptane
28	19.605	0.98	3,7-Dimethyl-2,6-octadien-1-yl acetate
29	19.746	1.05	2,6,6-Trimethyl-1-cyclohexen-1-yl ethanol
30	20.085	5.09	3-Tetradecanynoic acid
31	20.119	2.72	1,1,7-Trimethyl-4-methylenedecahydrocyclopropaazulene
32	20.215	1.85	trans-Bisabolene epoxide
33	20.637	8.64	5-Trimethyl-5-vinyltetrahydrofuran-2-methanol
34	21.368	1.97	2-Bicyclonon-6-en-3-yl-propan-2-ol
35	21.600	0.86	2-Isopropylidene-5-methylhex-4-enal
36	21.696	1.07	3,7,11-Trimethyl-6,10-dodecadien-1-yn-3-ol
37	21.838	1.38	n-Hexadecanoic acid
38	23.456	1.10	1-Dodec-9-yn-1-yl 4-hexyl butanedioate

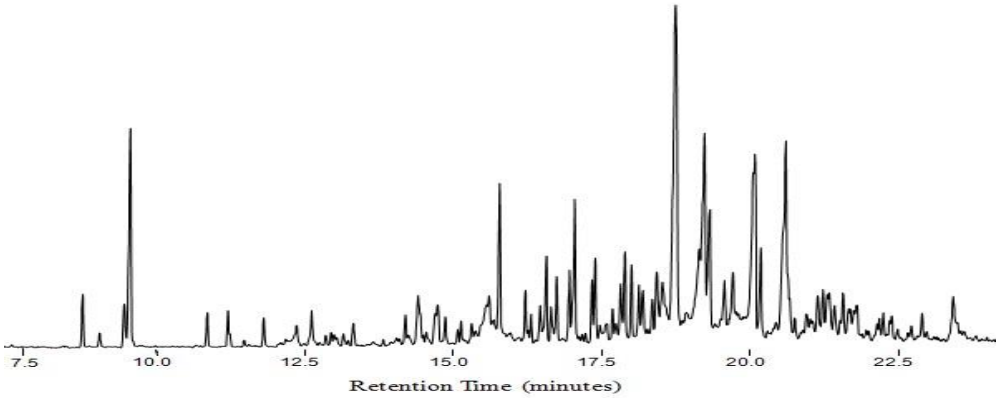

Figure 1. Chromatogram of chloroform seed extract of *S. molle.*

4. Conclusion

We identified the phytochemical compositions present in the chloroform seed extract of *S. molle* collected from the Kingdom of Lesotho by GC-MS analysis. To the best of our knowledge this is the first report of this kind on the chloroform seed extract of *S. molle*.

Conflict of interest

The authors declare no conflict of interest, financial or otherwise.

Acknowledgements

The authors thank the support from National University of Lesotho (NUL).

References

[1] M. Mehani and L. Segni, *Int. J. Bio. Life Sci.*, **2013**, 7(12), 1036–1038.

[2] N. M. R. Pedro, M. R. Jesus, D. David, M. S. G. Heriberto, A. S. Lucia and B. P. Eunice, *Molecules.* **2012**, 17(10), 12023–12036.

[3] T. N. Trevor, M. Oscar, S. Amidou, C. Eliton, H. E. Kennedy, B. G. Mazuru, L. M. Michael and M. Perkin, *Afr. J. Biotechnol.*, **2013**, 12(8), 854–859.

[4] A. Abderrahim, K. Belhamel, P. Chalard and G. Figueredo, *J. Food Measure. Char.*, **2018**, 12(2), 1123–1134.

[5] O. Deveci, A. Sukan, N. Tuzun, E. Esin, and H. Kocabas, *J. Med. Plant. Res.*, **2010**, 4, 2211–2216.

[6] C. Diaz, S. Quesada, O. Brenes, G. Aguilar and J. F. Ciccio, *Nat. Prod. Res.*, **2008**, 22, 1521–1534.

[7] A. A. Ferrero, J. O. W. Gonzalez and C. S. Chopa, *Fitoterapia.* **2006**, 77(5), 381–383.

[8] M. J. Ruffa, G. Ferraro, M. L. Wagner, M. L. Calcagno, R. H. Campos and L. Cavallaro, *J. Ethnopharmacol.*, **2002**, 79, 335–339.

[9] Z. Yueqin, M. C. Recio, S. Manez, R. M. Giner, M. Cerda-Nicolas and J. L. Rios, *Plant Med.*, **2003**, 69, 893–898.

[10] K. Abir, H. Majdi, A. Manef and A. Sameh, *J. Chem. Pharm. Res.*,**2016**,8(5), 93–101.

[11] H. Bendaoud, M. Romdhane, J. P. Souchard, S. Cazaux and J. Bouajila, *J. Food. Sci.*, **2010**, 75(6), C466–C472.

[12] Z. M. S. Mohamed, Z. Z. Mohamed, M. A. Hayssam and S. M. A. Mamoun, *J. Wood Sci.*, **2016**, 62, 548–561.

[13] K. Belhamel and L. R. Abderrahim, *Int. J. Essent. Oil Ther.*, **2008**, 2, 175–177.

[14] K. Hosni, M. Jemli, S. Dziri, Y. M'rabet, A. Ennigrou, A. Sghaier, H. Casabianca, E. Vulliet,N. B. Brahim and H. Sebei, *Ind. Crops Prod.*, **2011**, 34, 1622–1628.

[15] A. C.do Prado, H. G. Garces, E. Bagagli, V. L. M. Rall, A. Furlanetto, J. A. Fernandes and F. B. Furtado, *J. Appl. Microbiol.*, **2018**, doi: 10.1111/jam.14157.

[16] J. A**.** Duarte, L. A. B. Zambrano, L. D. Quintana, M. B. Rocha, E. G. Schmitt, A. A. Boligon, M. M. Anraku de Campos, L. F. S. de Oliveira and M. M. Machado, *Evid. Based Complement. Alternat. Med.*, **2018**, 6541583, 1-9.

[17] S. Garzoli, M. V. Laghezza, G. Turchetti, L. Pesci, A. Tiezzi and E. Ovidi, *Nat. Prod. Res.*, **2018**, 29, 1-4.

[18] C. Rey-Valeirón, K. Pérez, L. Guzmán, J. López-Vargas and E. Valarezo, *Exp. Appl. Acarol.*, **2018**, 76(3), 399-411.

Phytochemical characterization of essential oils from shoots, mature leaves and branchlets of *Litsea elliptica* (Lauraceae) collected in Brunei Darussalam

Manoharan Karuppiah Pillai[1,2], Farazimah binti Hj Yakop[1], Nurzaidah binti Metussin[1], Malai Haniti binti Sheikh Abd Hamid[1], Hartini binti Hj Mohd Yasin[1], Hj Mohamed bin Hj Abdul Majid[1] and David James Young[1,3,4]**

[1]*Faculty of Science, Universiti Brunei Darussalam, Jalan Tungku Link, Gadong BE 1410, Brunei Darussalam*
[2]*Faculty of Science and Technology, Department of Chemistry and Chemical Technology, National University of Lesotho, Roma Campus, P. O. Roma 180, Kingdom of Lesotho, Southern Africa*
[3]*School of Science, Monash University Malaysia, 47500 Bandar Sunway, Selangor D.E, Malaysia*
[4]*College of Engineering, Information Technology and Environment, Charles Darwin University, Darwin, NT 0909, Australia*

**corresponding author emails: david.young@cdu.edu.au, mohamed.majid@ubd.edu.bn*

Abstract

Essential oils from shoots, mature leaves and branchlets of *Litsea elliptica* were analyzed for their phytochemical compositions by GC-MS. A total of 12 compounds were identified from all three essential oils of *L. elliptica*.7-Decen-2-one (44.60%), 9-decen-2-ol (23.65%) and 2,7-octadienyl acetate (13.80%) were the major constituents of the essential oil from the shoots. *p*-Menthan-8-ol, (18.57%), 7-decen-2-one (10.62%), 9-decen-2-ol (25.09%) and α-terpineol (34.54%) were the major constituents of the essential oil from the mature leaves. Geranyl acetate (58.51%) and α-terpineol (20.95%) were the major constituents of the essential oil from the branchlets. *L. elliptica* has therapeutic applications in traditional medicine. Essential oils and/or extracts from various parts of this plant are reported to have promising biological and pharmacological activities.

Index Terms: Litsea elliptica, Litsea, Lauraceae, essential oils, GC-MS analysis, phytochemical compositions

1. Introduction

The species *Litsea elliptica* belongs to the Lauraceae family of the genus *Litsea*. *L. elliptica* is widely distributed in Southeast Asia.[1] This plant has therapeutic applications in traditional medicine.[2-5] In Brunei Darussalam, the leaves of *L. elliptica* are often mixed in salad and consumed. Essential oils, extracts and/or pure compounds from *L. elliptica* showed larvicidal,[6] adulticidal,[7] insecticidal,[8] anti-diarrheal,[9] anti-microbial,[10,11] phytopesticidal,[12] antimutagenicity[13] and anti-HIV activities.[14,15] *L. elliptica* has also been evaluated for its toxic effect on red blood cells of Sprague-Dawley rats[5] and acute and sub-acute oral toxicities in female Sprague-Dawley rats.[16] To date, the phytochemical compositions of the essential oils from *L. elliptica* have not been reported. The aim of the present study is to determine the phytochemical compositions of essential oils from shoots, mature leaves and branchlets of *L. elliptica* collected in Brunei Darussalam by GC-MS analysis. The results thus obtained are communicated in this article.

2. Experimental Method

2.1 Plant materials

Samples of shoots, mature fresh leaves (75 g each) and branchlets (53 g) of *L. elliptica* were collected in December 2013 near Kuala Lurah (Brunei Darussalam). The plant material was identified by Prof. Dato Hj. Mohamed bin Hj. Abdul Majid, Department of Biological Sciences, Universiti Brunei Darussalam. Voucher specimens for the shoots (UBD/BRC/6/LE-SHOOTS), mature leaves (UBD/BRC/6/LE-LEAF-M) and branchlets (UBD/BRC/6/LE-STEM) were deposited at the Herbal Drug Discovery Laboratory, Universiti Brunei Darussalam.

2.2 Processing plant materials

The shoots and mature fresh leaf samples of *L. elliptica* were cut into small pieces using scissors. The branchlets of *L. elliptica* were first chopped into small pieces and then ground into coarse powder using a blender equipped with a mill attachment (HR2116, Philips, Amsterdam, Netherlands).

2.3 Preparation of essential oils

The prepared shoots, mature leaves and branchlet samples were placed in separate 250 mL round-bottom flasks containing 200 mL water and subjected for steam distillation at 110–120°C for 3 hours. 0.87, 0.87 and 0.08 g of essential oils were obtained from shoots, mature leaves and branchlets, respectively. The essential oils were dried over anhydrous Na_2SO_4 and then used for GC-MS analysis.

2.4 Analysis of essential oils

GC-MS analysis of the essential oils was carried out on GC-2010 (Shimadzu, Kyoto, Japan) equipped with a MS-QP2010 mass spectrometer and a DB-5 column (30 m × 0.25 mm, i.d., 0.25 µm film thickness). The following temperature program was used: 50°C, held for 1 minute; increased to 140°C at 20° C/minute; increased to 300°C at 10°C/minute and held for 10 minutes. The total run time was 31.5 minutes. Helium was used as the carrier gas at a flow rate of 1.69 mL/minutes. The injector port temperature was 250ºC. For sample preparation, 0.05 mL of the essential oil sample was diluted in 5 mL of hexane and 1.0 µL was injected in split less mode. The MS operating parameters were as follows: interface temp. 250ºC; ion source temp. 200º C; electron energy for electron ionization, 70 eV; accelerating voltage relative to the tuning result, −0.10 kV gain; scan range, *m/z* 0–250; and scan rate, 526/sec. The solvent cutoff was at 3 minutes.

2.5 Identification of chemical compositions

The chemical compositions in the essential oils were identified using their retention indices with reference to a homologous series of n-alkanes (C8–C14, PolyScience, Niles.IL) and by comparison of their MS spectra with NIST/EPA/NIH/NIST08 library data. Additionally, their retention indices were also compared with literature values.[31-35]

3. Results and Discussion

The phytochemical compositions of essential oils from shoots, mature leaves and branchlets of *L. elliptica* were determined by GC-MS. A total of 12 compounds were identified in all three essential oils from *L. elliptica* and they are *p*-menthan-8-ol (**1**), citronellal (**2**), 7-decen-2-one (**3**), 9-decen-2-ol (**4**), α-terpineol (**5**), 2-decanol (**6**), 2,7-octadienyl acetate (**7**), *trans*-dihydrocarvone (**8**), 8-methylnonanane-1,8-diol (**9**), 2-methylundecanal (**10**), geranyl acetate (**11**) and 2-dodecanone (**12**). All these compounds are listed in ***Table 1*** in the order of their elution along with the relative percentage and retention time. The chromatograms of the essential oils are also given in ***Figure 1(A)***, ***(B)***, and ***(C)*** for the shoots, mature leaves and the branchlets, respectively.

The major components in the essential oil from shoots were **3** (44.60 %), **4** (23.65%) and **7** (23.65%) and together they accounted more than 82% of the total essential oil. The major components identified in the essential oil from mature leaves were **1** (18.57%), **3** (10.62%), **4** (25.09%) and **5** (34.54%) and together they accounted more than 88% of the total essential oil.**11** (58.51%) and **5** (20.95%) were the main

components identified in the essential oil from the branchlets and together they accounted about 80% of the total essential oil. Although **11** was a major component identified in the essential oil from branchlets, it was either absent or present in a negligibly small quantity in the essential oils from shoots and mature leaves (refer to ***Table 1***). Similarly, **3** was identified as a major component (44.60%) in the essential oil from shoots but it was present only at low levels (10%) in the essential oil from mature leaves. The essential oil from branchlets has no trace of **3** (refer to ***Table 1***). Compound **4** was one of the major components in the essential oils from both the shoots and mature leaves (23.65% and 25.09%, respectively) but it was present only at low levels (3.15%) in the essential oil from branchlets. Compound **11** is one of the most frequently encountered compounds in many essential oils from various plants and those essential oils with **11** as one of the components exhibited significant antioxidant activity in the DPPH radical scavenging assay.[22-24] Our literature search showed that *L. elliptica* has not been investigated extensively for its phytochemical constituents. Undec-10-en-12-one, tridec-12-en-2-one and (+)-reticuline have previously been reported from the bark of *L. elliptica*.[25] However, alkaloids,[26-29] terpenes,[28-31] flavonoids,[26,28 29] steroids,[28,29,32,33] lactones,[28,29,34,35] amides,[28,29,36,37] fatty acids,[28, 29,38,39] etc. classes of compounds have been reported from many other species of the genus *Litsea*.

Table 1.Phytochemical compositions of essential oils extracted from shoots, mature leaves and branchlets of *L. elliptica*.

Compound No.	$RI_{Exp.}$	RI_{Lit}	New leaves (%) & (Rt)	Mature leaves (%) & (Rt)	Branchlets (%) & (Rt)
1	1145	1144	1.10 (6.601)	18.57 (6.602)	3.83 (6.601)
2	1154	1153	-	1.08 (6.676)	1.91 (6.675)
3	1160	1159	44.60 (6.739)	10.62 (6.734)	-
4	1170	1168	23.65 (6.808)	25.09 (6.811)	3.15 (6.813)
5	1176	1174	8.44 (6.857)	34.54 (6.858)	20.95 (6.857)
6	1179	1178	0.92 (6.883)	3.94 (6.883)	1.58 (6.883)
7	1192	1181	13.80 (7.001)	1.59 (7.000)	-
8	1201	1201	5.58 (7.079)	1.03 (7.077)	-
9	1346	1350	-	-	3.76 (8.492)
10	1365	1366	-	1.18 (8.674)	4.57 (8.675)
11	1376	1383	-	0.81 (8.781)	58.51 (8.784)
12	1395	1396	1.92 (8.972)	1.56 (8.971)	1.74 (8.973)

Numbers in brackets are retention times (Rt) (minutes); $RI_{Exp.}$= experimental retention indices; $RI_{Lit.}$= literature retention indices.[17-21]

4. Conclusion

We identified the phytochemical compositions present in essential oils of shoots, mature leaves and branchlets of *L. elliptica* collected in Brunei Darussalam by GC-MS analysis. To the best of our knowledge this is the first report of this kind on essential oils from shoots, mature leaves and branchlets of *L. elliptica*.

Conflict of interest

The authors declare no conflict of interest, financial or otherwise.

Acknowledgements

This work was supported by the Department of Economic Planning and Development (JPKE) through the Brunei Research Council under Grant No. UBD/BRC/6.

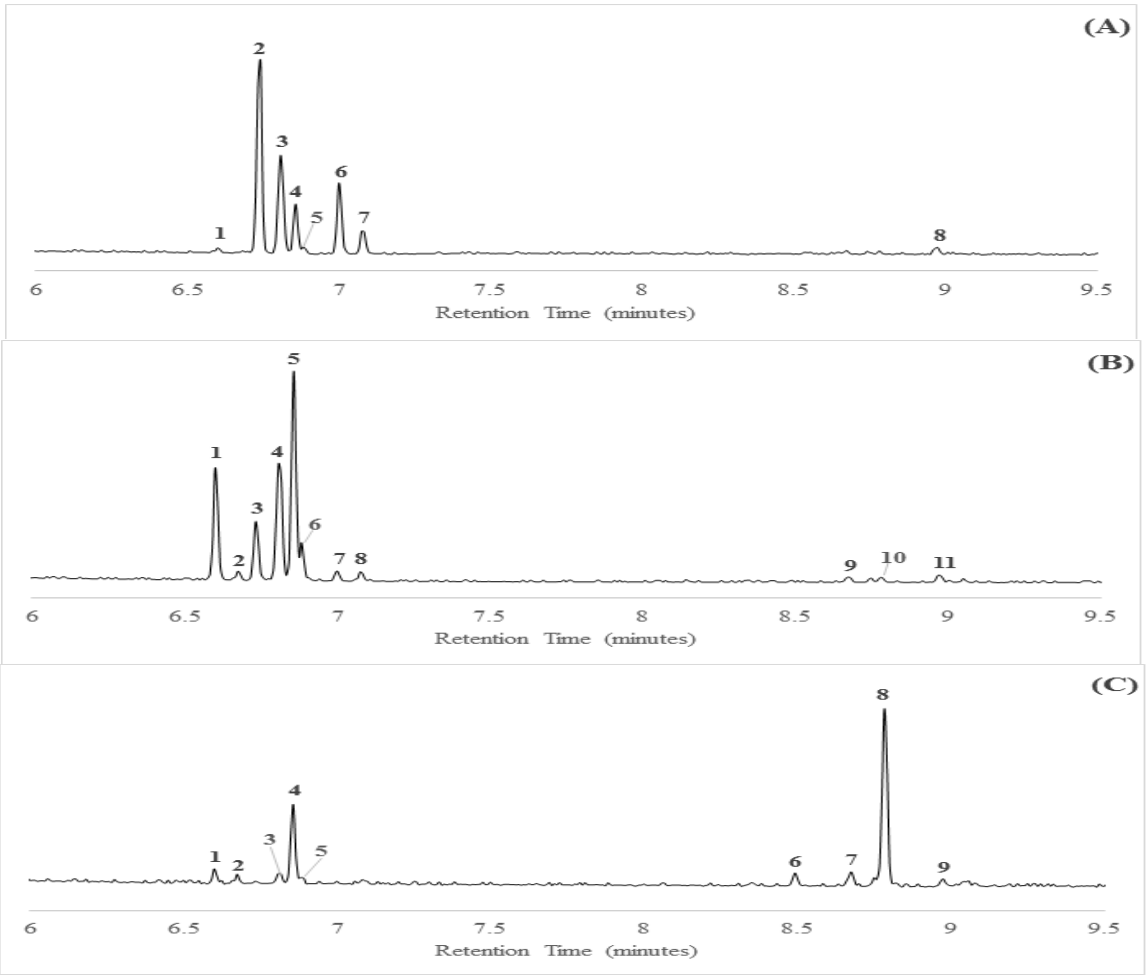

Figure 1. Chromatograms of essential oils from the shoots, mature leaves and branchlets of *L. elliptica*. Chromatogram (**A**) for shoots, (**B**) for mature leaves and (**C**) for branchlets.

References

[1] S. Jiwajinda, V. Santisopasri, A. Murakami, M. Kawanaka, H. Kawanaka, M. Gasquet, R. Eilas, G. Balansard and H. Ohigashi, *J. Ethnopharmacol.,* **2002**, 82(1), 55–58.

[2] J.Suratwatdee, S. Vilai, M. Akira, K. Oe-Kyung, H. W. Kim and H. Ohigashi, *J. Cancer Prev.*, **2002**, 3, 215–223.

[3] P. W.Grosvenor, P. K. Gothard, N. C. McWilliam, A. Supriono and D. O. Gray, *J. Ethnopharmacol.*, **1995**, 45, 75– 95.

[4] S. Bhamarapravati, S. L. Pendland and G. B. Mahady, *In Vivo*, **2003**, 17(6), 541–544.

[5] T. I. Shima, B. S. Balkis, S. N. A. S Maseran, J. Mohamed, S. R. Louis, S. Das, S. Sellehudin, N. R. Rajab and H. Othman, *J. Zhejiang Univ. Sci.*, **2009**, 10(11), 813–819.

[6] O. Hidayatulfathi, S. Sallehudin, J. Ibrahim and A. K. Azizol, *Trop. Biomed.*, **2003**, 20(2), 153–157.

[7] O. Hidayatulfathi, S. Sallehudin and J. Ibrahim, *Trop. Biomed.*, **2004**, 21(2), 61–67.

[8] R. Rohani, W. A. Nazni, L. V. Ngo, J. Ibrahim and H. L. Lee, *Trop. Biomed.*, **1997**, 14, 5–9.

[9] P. S. Poonia, D. Samuel and P. M. Mazumdar, *Fitoterapia.* **2007**, 78, 171–174.

[10] S. Y. Lee, B. S. Min ,J. H. Kim, J. Lee, T. J. Ki, C. S. Kim, Y. H. Kim and H. K. Lee, *Phytother. Res.*, **2005**, 19, 273–276.

[11] S. C. Mandal, C. K. Kumar, R. Majumader and B. C. Maity, *Fitoterapia.* **2000**, 71, 439–441.

[12] S. Pukhan and M. C. Kalita, *Indian J. Exp. Biol.*, **2005**, 43, 472–474.
[13] K. Nakahara, G. Trakoontivakom, N. S. Alzoreky, H. Ono, M. Onishi-Kameyama and M. Yashida, *J. Agric. Food. Chem.*, **2002**, 50, 4796–4802.
[14] V. D. Hoang, G. T. Tan, H. J. Zhang, P. A. Tamez, V. V. Hung, N. M. Cuong, D. D. Socjarto, H. H. Fongand J. M. Pezzuto, *Phytochemistry*. **2002**, 59, 25–329.
[15] H. J. Zhang, V. H. Nguyen, M. C. Nguyen, D. D. Soejarto, J. M. Pezzuto, H. H. Fong and G. T. Tan, *Planta Med.*, **2005**, 71, 452–457.
[16] B. S. Balkis, S. N. A. S. Maseran, O. Baharuddin, T. I. Shima and H. Othman, *J. Zhejiang Univ. Sci.*, **2012**, 13(10), 783–790.
[17] R. P. Adams, *Biochem. Syst. Ecol.*, **1999**, 27, 709–725.
[18] R. P. Adams, *Biochem. Syst.Ecol.*, **2000**, 28(6), 515–528.
[19] C. Economakis, H. Skaltsa, C. Demetzos, M. Sokovic and C. A. Thanos, *J. Agric. Food. Chem.*, **2002**, 50(22), 6276–6280.
[20] S. R. Lee, C. Macku and T. Shibamoto, *J. Agric. Food. Chem.*, **1991**, 39(11), 972–975.
[21] K. Javidnia, R. Miri, M. Kamalinejad and A. Nasiri, *Flavour Fragr. J.*, **2002**, 17, 465–467.
[22] A. K. Pandey, The Cymbopogons-Harvest and postharvest management. In: A. Akhila (Ed.), Essential oil-bearing grasses-The genus Cymbopogon: Medicinal and Aromatic Plants-Industrial Profiles. CRC Press, Boca Raton, **2010**, p.118.
[23] M. N. Dib, M. El-Amine, A. Hocine and T. Boufeldja, *Int. Res. J. Biological Sci.*, **2013**, 2(1), 22–29.
[24] H. H. A. El-Baky and G. S. El-Baroty, *IJIB*, **2008**, 3(3), 202–208.
[25] D. Arbain, N. Dasma, S. Ibrahim and M. V. Sargent, *Aust. J. Chem.*, **1990**, 43(11), 1949-1952.
[26] R. Liu, H. E. Zhang, F. Zhou, R. M. Wang, Q. Tu and J. Y. Wang, *Syst. Ecol.*, **2013**, 50, 293-295.
[27] W. Zhan, J. F. Hu, W. W. Lu, Q. C. Zhao and G. B. Shi, *Molecules*, **2012**, 12950-12960.
[28] Y.S. Wang, Z, Q. Wen, B. T. Li, H. B. Zhang and J. H. Yang. *J. Ethnopharmacol.* 2**016**, 181, 66-107.
[29] D. G. Kong, Y. Zhao, G. H. Li, B. J. Chen, X. N. Wang, H. L. Zhou, H. X. Lou, D. M. Ren and T. Shen, *J. Ethnopharmacol.*, **2015**, 164, 256-264.
[30] Y. S. Wang, R. Huang, Y. Li, W. B. Shang, F. Chen, H. B. Zhang and J. H. Yang, *Phytochem. Lett.*, **2013**, 6, 26-30.
[31] L. Si, Y. Chen, X. Han, Z. Zhan, S. Tian, Q. Cui and Y. Wang, *Molecules*, **2012**, 17, 7057-7066.
[32] Y. Xiao, J. F. Zhao, X. D. Yang, R. Huang and W. Li, *Acta. Bot. Yunnanica*, **2005**, 27, 695-697.
[33] L. L. Tsai, I. I. Lai-Yuan, C. Y. Duh, Y. F. Jeng and I. S. Chen, *Chin. Pharm. J.*, **2000**, 52, 235-239.
[34] K. Takeda, K. Sakurawi and H. Ishii, *Tetrahedron*, **1972**, 28, 3757-3766.
[35] N. Agrawal, A. S. Choudhary and M. C. Sharma and M. P. Dobhal, *Chem. Biodiverse.*, **2011**, 8, 223-243.
[36] Q. Guo, K. W. Zeng, X. L. Gao, Z. X. Zhu, S. Y. Zhang, X. Y. Chai and P. F. Tu, *J. Nat.Med.*, **2015**, 69, 94-99.
[37] P. C. Pan, M. J. Cheng, C. F. Peng, H. Y. Huang, J. J. Chen and T. S. Chan, *J. Nat. Med.*, **2010**, 73, 890-896.
[38] X. H. Yan, X. Y. Wei, H. H. Xie, M. F. Liu and F. X. Zhang, *J. Trop. Subtropical. Bot.*, **2000**, 8, 171-176.
[39] J. U. Choudhury, N. I. Bhuiyan and N. C. Nandi, *J. Bot.*, **2008**, 37, 81-83.

Optimization of Rock Physics Models by Combining the Differential Effective Medium (DEM) and Adaptive Batzle-Wang Methods in "R" Field, East Java

M. Wahdanadi Haidar[1], Reza Wardhana[2], M. Iksan[2], and M. Syamsu Rosid[2]*

[1]JOB – Pertamina Petrochina East Java, Menara Kuningan Lt. 18 & 20, Jakarta 12940, Indonesia
[2]Geophysics, FMIPA Universitas Indoesia, Depok 16424, Indonesia

**corresponding author email: syamsu.rosid@ui.ac.id*

Abstract

The pore systems in carbonate reservoirs are more complex than the pore systems in clastic rocks. There are three types of pores in carbonate rocks: interparticle pores, stiff pores and cracks. The complexity of the pore types can lead to changes in the P-wave velocity by up to 40%, and carbonate reservoir characterization becomes difficult when the S-wave velocity is estimated using the dominant interparticle pore type only. In addition, the geometry of the pores affects the permeability of the reservoir. Therefore, when modelling the elastic modulus of the rock it is important to take into account the complexity of the pore types in carbonate rocks. The Differential Effective Medium (DEM) is a method for modelling the elastic modulus of the rock that takes into account the heterogeneity in the types of pores in carbonate rocks by adding pore-type inclusions little by little into the host material until the required proportion of the material is reached. In addition, the model is optimized by calculating the bulk modulus of the fluid filler porous rock under reservoir conditions using the Adaptive Batzle-Wang method. Once a fluid model has been constructed under reservoir conditions, the model is entered as input for the P-wave velocity model, which is then used to estimate the velocity of the S-wave and the proportion of primary and secondary pore types in the rock. Changes in the characteristics of the P-wave which are sensitive to the presence of fluid lead to improvements in the accuracy of the P-wave model, so the estimated S-wave velocity and the calculated ratio of primary and secondary pores in the reservoir are more reliable.

Index Terms: carbonate reservoir, Differential Effective Medium (DEM), Adaptive Batzle-Wang, optimization, pore type

1. Introduction

Carbonate reservoirs are one of the principal types of oil- and gas-producing reservoirs worldwide. Unfortunately, carbonate rocks are more complicated in structure than siliciclastic rocks, with the result that carbonate reservoirs are usually harder to model than sand reservoirs. The primary difference between carbonate reservoirs and sand reservoirs is the distance traveled before deposition. Whereas carbonate rocks are formed by local deposition, the grains that comprise siliciclastic rocks may travel hundreds of miles down river systems before deposition and lithification. The fact that deposition is local significantly affects the heterogeneity of carbonate rocks.

One of the methods that is commonly used to characterize carbonate reservoirs is rock physics analysis. This method can be used to calculate the often very complex mix of pore types in carbonate rocks from their elastic moduli. In terms of their geophysics, the porosities in carbonate rocks can be divided into three types: interparticle or reference pores, which separate the carbonate grains and are considered to be the dominant pore types in carbonates; vuggy pores, which represent moldic and stiff pores and are

usually formed as a by-product of the dissolution of grains and fossil chambers; and cracks, which represent micro-fractures and micro-cracks.

There are several methods available for calculating the quantity and distribution of pore types in carbonate reservoirs. These include the Self-Consistent (SC), Kuster-Toksoz (KT), and Differential Effective Medium (DEM) methods. In a previous study, Rosid et al.[1] implemented the DEM method to characterize the pore types within a carbonate reservoir. Candikia et al.[2] have also compared the KT and DEM methods and they conclude that the Differential Effective Medium method is better than the Kuster-Toksoz method in generating the V_s log and determining the carbonate reservoir pore types. Therefore, we will use the DEM method to generate the pore logs and the V_s logs corresponding to the fluid conditions in the carbonate reservoir, by incorporating the physical parameters of the reservoir fluid as measured in situ and not taken from the literature. Our expectation is that the correlation coefficient between the P-wave velocity V_p predicted by the model and the measured values of V_p improves. The correlation should improve because the value of V_p is very sensitive to the presence of fluid in the reservoir, and the model can incorporate conditions that are closer to the actual situation in the "R" field.

The data used in this study were taken from three wells. The first well is called RZ-14, and information is available about the depth of this well, the values of the effective and total porosities, the water saturation, the mineral and fluid fractions, the primary velocity (V_p), the density and the shear wave velocity (V_s). The two other wells are called RZ-35 and RZ-09. The datasets for both of them cover the same parameters as for RZ-14, except for the values of *V*s which are not available for either well. The data is listed in ***Table 1***.

2. Methodology

2.1 Voigt-Reuss-Hill method

The Voigt-Reuss-Hill method is used to construct the background model of the mineral mix in the solid rock phase in the carbonate reservoir. This method is effectively an average of two precursor methods, namely the Voigt method which arranges the rock matrix in series and Reuss method which arranges the rock matrix in parallel. Constructing a model of the solid rock phase is only a first step in carbonate reservoir modelling, as it assumes that the rock has 0% porosity and so consists entirely of minerals such as clay, dolomite and calcite. The bulk and shear modulus of the solid rock phase are calculated using the Voigt-Reuss-Hill formulas shown below:[3]

Voigt Method

$$M_V = \sum_{i-n}^{N} f_i . M_i$$

where M_V : Voigt elastic modulus
f_i : mineral fraction
M_i : elastic modulus of mineral

Reuss Method

$$\frac{1}{M_R} = \sum_{i-1}^{N} \frac{f_i}{M_i}$$

where M_R : Reuss elastic modulus
f_i : mineral fraction
M_i : elastic modulus of mineral

Voigt-Reuss-Hill Method

$$M_{VRH} = \frac{M_V + M_R}{2}$$

where M_V : Voigt elastic modulus
M_R : Reuss elastic modulus
M_{VRH} : Voigt-Reuss-Hill elastic modulus

2.2 Adaptive Batzle-Wang method

The Adaptive Batzle-Wang method is our modification of the standard Batzle-Wang method. The advantages of this method is that it can be adjusted to the field conditions in the location where the study is being performed. As a result, the fluid parameters can be chosen to be close to the reservoir conditions in that field. In the Adaptive method, the elastic parameters of the fluids are not necessarily the same at each depth and the distributions of the individual bulk moduli such as K_{water}, K_{oil}, and K_{gas} can be inserted in Wood's formula to calculate the bulk modulus of the fluid mixture at each depth in the reservoir. If we were not using Adaptive Batzle-

Wang method the elastic parameters of the fluids would be the same at each depth and the Differential Effective Medium method would not be optimized for the conditions in the reservoir.

Table 1. Availability of petrophysics data.

Parameter	RZ-14	RZ-09	RZ-35
Depth	√	√	√
Effective Pore	√	√	√
Total Pore	√	√	√
Water Saturation	√	√	√
Mineral Fraction	√	√	√
Fluid Fraction	√	√	√
V_p	√	√	√
V_s	√	X	X
Density	√	√	√

2.3 Wood's formula

Wood's formula is used to calculate a value for the mixed bulk fluid modulus at each depth in each well. The individual values of the bulk moduli for water, oil and gas are usually taken from the literature. But in order to optimize the DEM method for the conditions in the reservoir the elastic parameters of the fluids are calculated in advance using the Adaptive Batzle-Wang method and then entered into Wood's formula. The elastic modulus of the fluid mixture is calculated from the equation below:[3]

$$\frac{1}{K_{FL}} = \frac{S_{Water}}{K_{Water}} + \frac{S_{Oil}}{K_{Oil}} + \frac{S_{Gas}}{K_{Gas}}$$

where, K_{FL} : elastic modulus of fluid mixture
S_{water} : water saturation
S_{oil} : oil saturation
S_{gas} : gas saturation
K_{water} : water bulk modulus
K_{oil} : oil bulk modulus
K_{gas} : gas bulk modulus

2.4 Differential Effective Medium method

A common method used to model the elastic properties of a porous rock is the DEM (Differential Effective Medium) method. The principle behind the DEM method is that a two-phase composites can be constructed by incrementally adding a small fraction of pores to the rock matrix. In the DEM method, the effective moduli depend on the path taken to construct the final composite. In effect, the DEM method works by inserting inclusions into the background model, with the model continuously changing as the inclusions are added:[3]

$$(1-y)\frac{d}{dy}\left[K^*(y)\right] = (K_2 - K^*)P^{(*2)}(y)$$

$$(1-y)\frac{d}{dy}[\mu^*(y)] = (\mu_2 - \mu^*)Q^{(*2)}(y)$$

where y : porosity
$K^*(y)$: the effective bulk moduli of DEM
K^* : bulk moduli of matrix (phase 1)
K_2 : bulk moduli of inclusion (phase 2)
$P^{(*2)}$: geometry factor for an inclusion of material 2 in a background medium with effective moduli K^* and μ^*
$\mu^*(y)$: the effective shear moduli of DEM
μ^* : shear moduli of matrix (phase 1)
μ_2 : shear moduli of inclusion (phase 2)
$Q^{(*2)}$: geometry factor for an inclusion of material 2 in a background medium with effective moduli K^* and μ^*

The steps that are followed in the DEM method are not significantly different from those in the KT method. Like the KT method, the DEM method starts with a background rock matrix, the geometry factor, the elastic moduli of the inclusions and the fraction of inclusions as inputs. The difference between the methods lies in how these inputs are used. The background rock matrix is constructed using the Voight-Reuss-Hill method. Instead of looping the aspect ratio, the DEM method uses the value of the

aspect ratio as an input to generate the geometry factor. There are three aspect ratio values that need to be determined, namely the aspect ratios of the interparticle pores, the stiff pores and the cracks. These three values are fixed by the Zhao classification, which divides the values of the aspect ratio into three groups. The aspect ratio representing cracks ranges from 0.01-0.02, that for the interparticle pores ranges from 0.12-0.15, and that for the stiff pores varies between 0.7-0.8. The third step is to calculate the reference value of V_p with the assistance of the DEM equation, which depends on the aspect ratio of the interparticle pores, the fraction of inclusions or porosity, the elastic moduli of the rock matrix and the elastic moduli of the inclusions. The reference value of V_p acts as a controller, determining whether stiff pores or cracks are to be added to the rock matrix. If the reference value of V_p is lower than the measured value of V_p then stiff pores are added. But if the reference value of V_p is higher than the measured value of V_p then cracks are added to the matrix. Once the process is complete, the effective elastic moduli are calculated and compared with the actual data, so that the most representative model can be chosen.

3. Results and Discussion

The first step in the modelling process is to construct the background model using the Voight-Reuss-Hill method, from which we obtain the bulk and shear modulus of the solid rock phase under the assumption of 0% porosity. The values of the bulk and shear modulus of the solid rock phase are used as inputs to calculate the pore type inversion and estimate the value of V_s via the DEM method. The results of this step are shown in ***Figure 1***, ***Figure 2*** and ***Figure 3***.

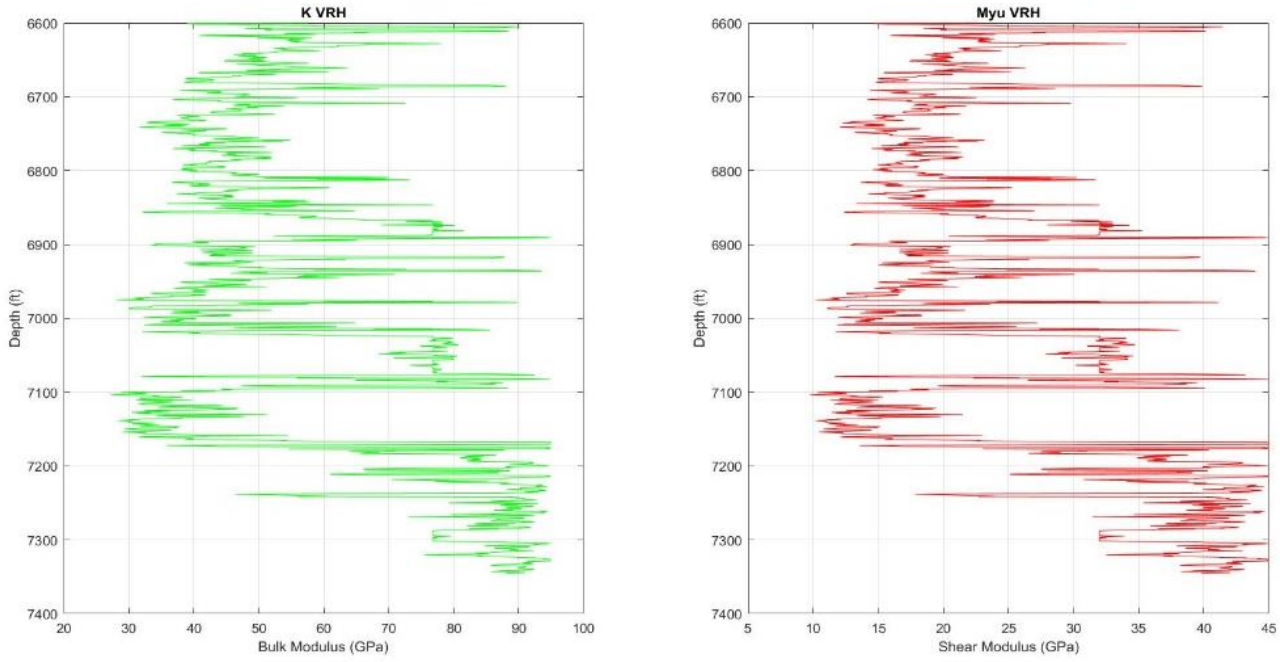

Figure 1. Bulk and shear modulus of solid rock model in RZ-14.

The fraction of secondary pore types - the stiff pores and cracks - is then calculated. The value of the S-wave velocity V_s in each well for which no V_s data is available is then estimated. In this step, we compare the results of the DEM method before and after optimization using the elastic moduli of the fluids generated by the Adaptive Batzle-Wang method. The Adaptive Batzle-Wang method is used to calculate the elastic moduli of the fluids at each depth under reservoir conditions, as shown in ***Figure 4***, ***Figure 5*** and ***Figure 6***.

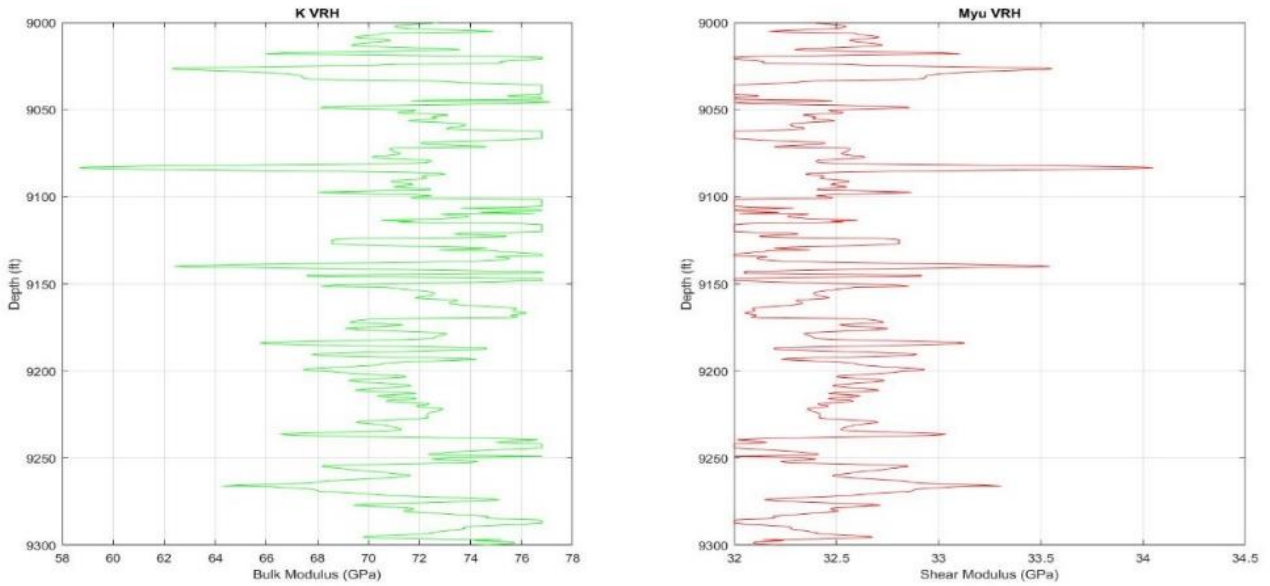

Figure 2. Bulk and shear modulus of solid rock model in RZ-09**.**

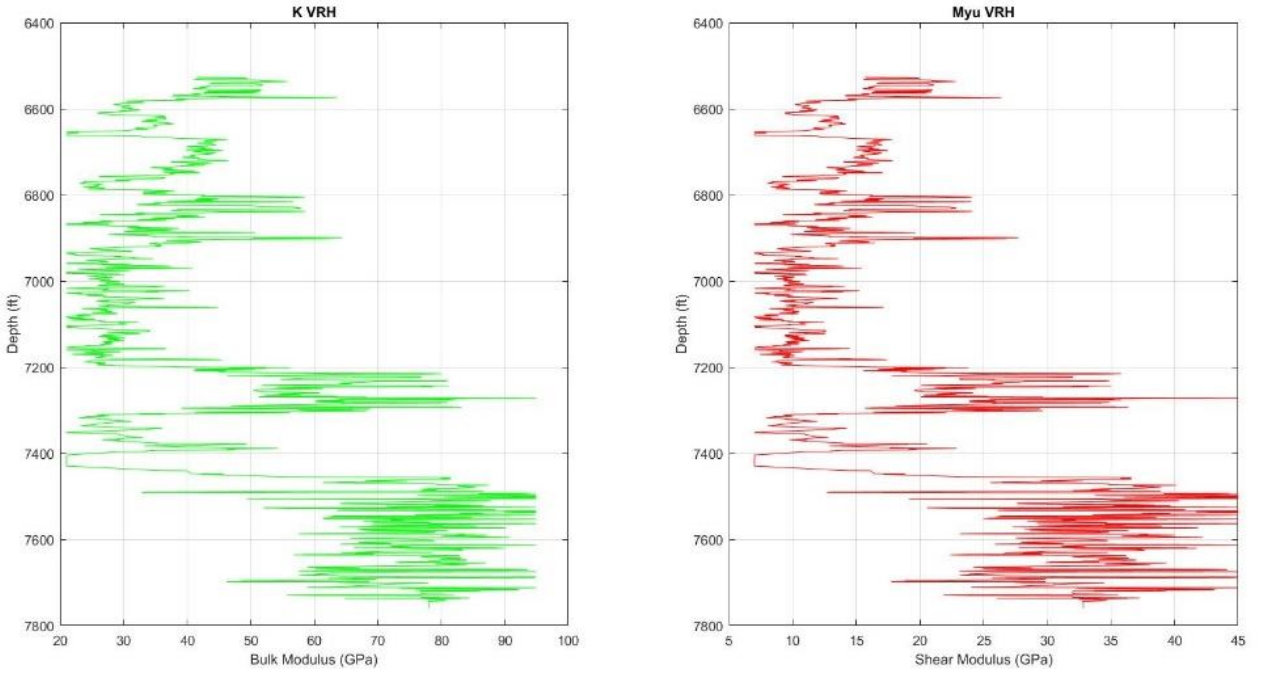

Figure 3. Bulk and shear modulus of solid rock model in RZ-35.

The fraction of secondary pore types and the estimated values of V_s in each well are then calculated using the DEM method. The DEM method models the porosities in the rocks. After applying this method, the likely pore types can be determined and the shear wave velocity can be estimated based on the effective moduli of the rocks. To determine the likely pore types, the inclusions are added to the rock matrix, after comparing the reference value of V_p to its measured value. To calculate the reference value of V_p we start with a rock~~s~~ model which contains 100% interparticle (dry rock) pores. The secondary pore type is added step by step, with a 1% fraction of inclusions added at each step to the dry rock model, until the value of V_p in the

model approaches the measured value of V_p. The value of V_p in the model is calculated using the DEM equation by inserting the effective bulk and shear modulus values into the equation for V_p, so as to ensure that the inclusion we add is of the appropriate type, as can be seen in ***Figure 7***, ***Figure 8*** and ***Figure 9***.

As can be seen in ***Figure 7***, the RMS error for RZ-14 decreases and the cross plot tends to be more linear after optimization because we have used more accurate input parameters. The more accurate input parameters we use, the more the RMS error value will decrease and the more accurate the calculated fraction of secondary pore types will be in each well.

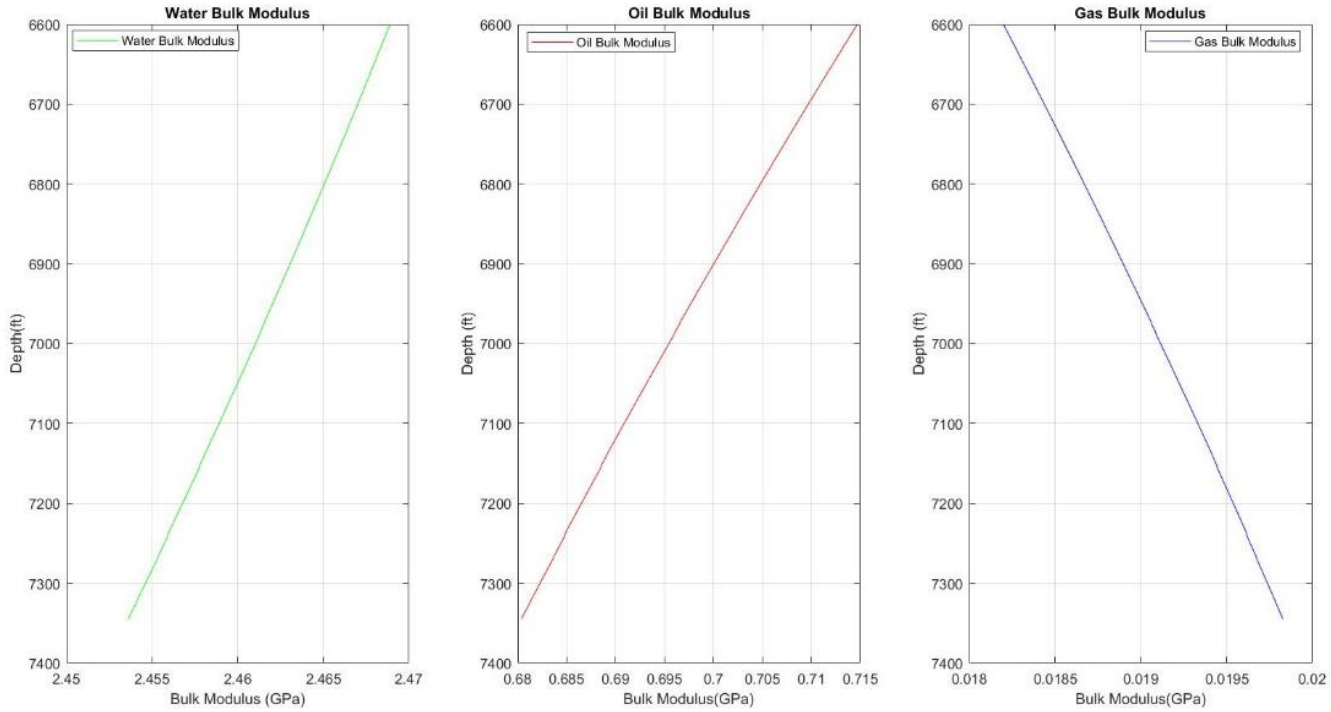

Figure 4. Bulk and shear modulus of solid rock model in RZ-35.

For well RZ-09, in ***Figure 8***, the DEM method is again successfully optimized and the RMS error decreases from 0.015256 to 0.015008. The final model should be a more accurate approximation to the actual conditions in the carbonate reservoir.

For well RZ-35, in ***Figure 9***, the model is again successfully optimized and the RMS error also decreases from 0.066157 to 0.065033, although there is still data scatter in the high clay zone. There is good reason to believe that there is no fluids content in the high clay zone, because of the impermeability of clay. So optimization using the Adaptive Batzle-Wang method may not be effective in the high clay zone.

We next compare the pore types calculated using the DEM method before and after optimization in ***Figure 10***. If we pay close attention to this figure, we can see the different fractions of secondary pore types before and after optimization. The differences are evident not only in the marked yellow boxes, but appear also along the whole range of well depths. The improved accuracy of the optimized pore type fractions is confirmed by the smaller RMS error in the cross plot between the value of V_p from the model and the measured value of V_p. However, in this figure the differences in the fractions of the secondary pore types are mostly not noticeable, unless we flip the image back onto itself.

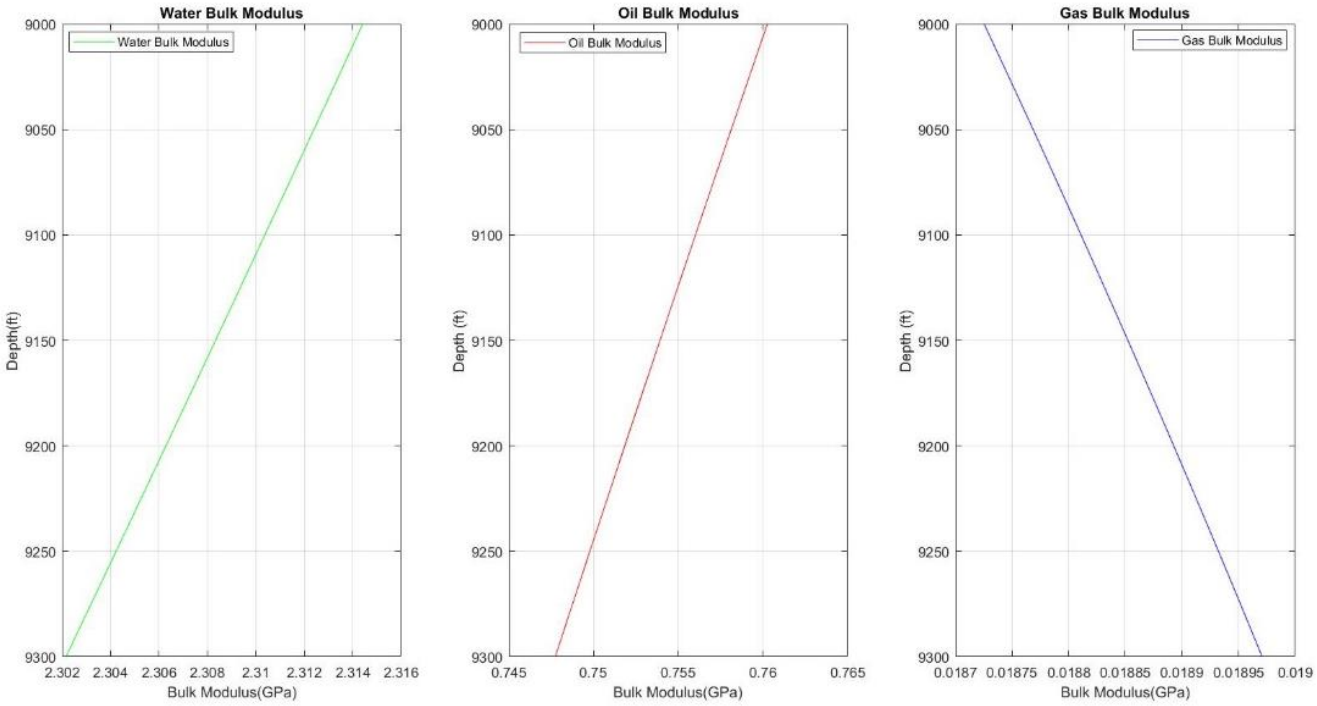

Figure 5. Elastic moduli of water, oil, and gas in RZ-09.

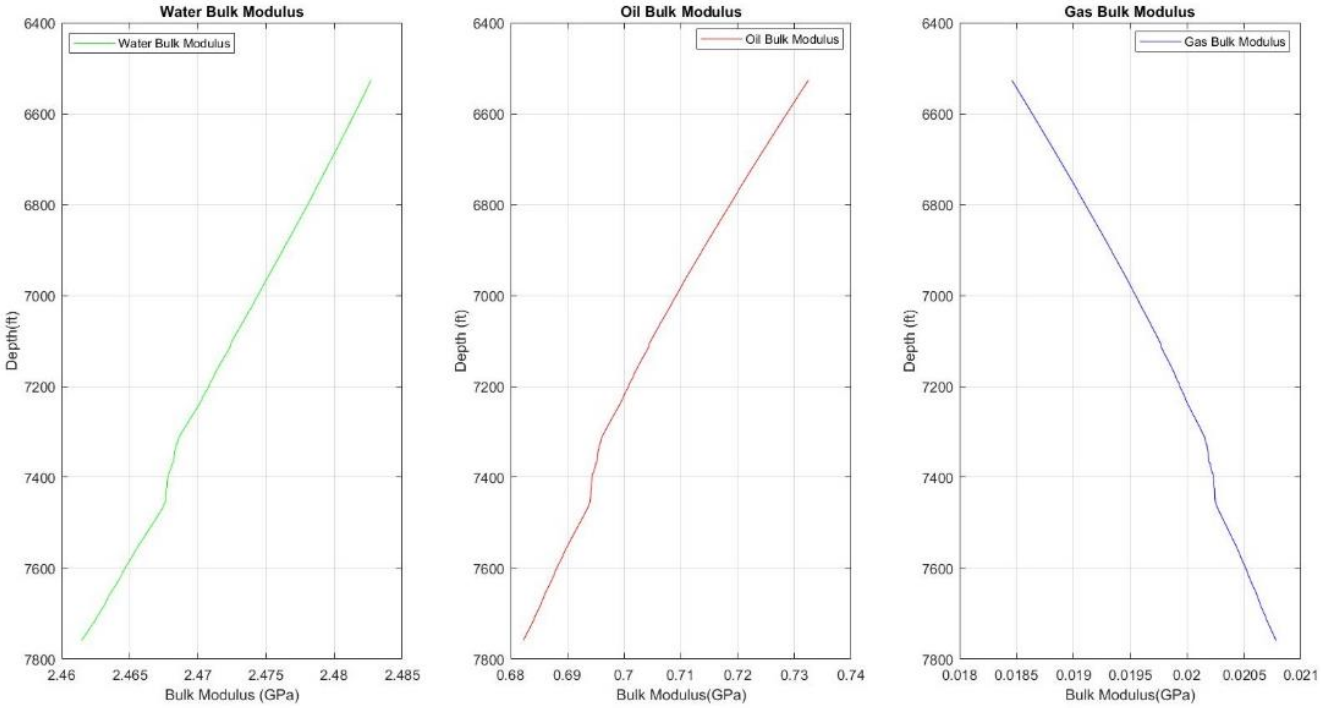

Figure 6. Elastic moduli of water, oil, and gas in RZ-35.

From ***Figure 14*** we can see the correlation coefficient between the values of V_p and V_s predicted by the model after optimization based on those results. ***Figure 14***, ***Figure 15*** and ***Figure 16*** show that the V_p – V_s trend has a quadratic correlation. The parabolic trend indicates that the reservoir in this research area is limestone, based on the Castagna's empirical V_p - V_s formula.[4]

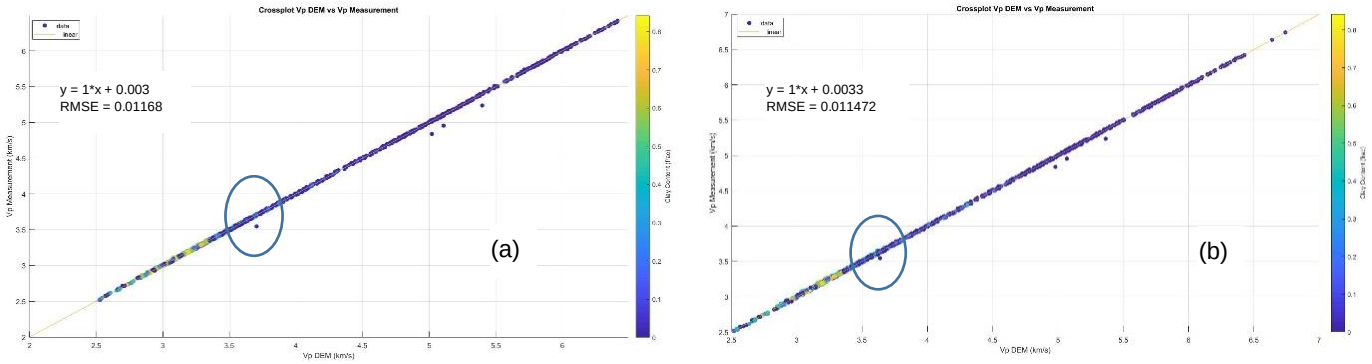

Figure 7. Cross plot between the value of V_p from the model and the measured value of V_p (a) before and (b) after optimization in RZ-14.

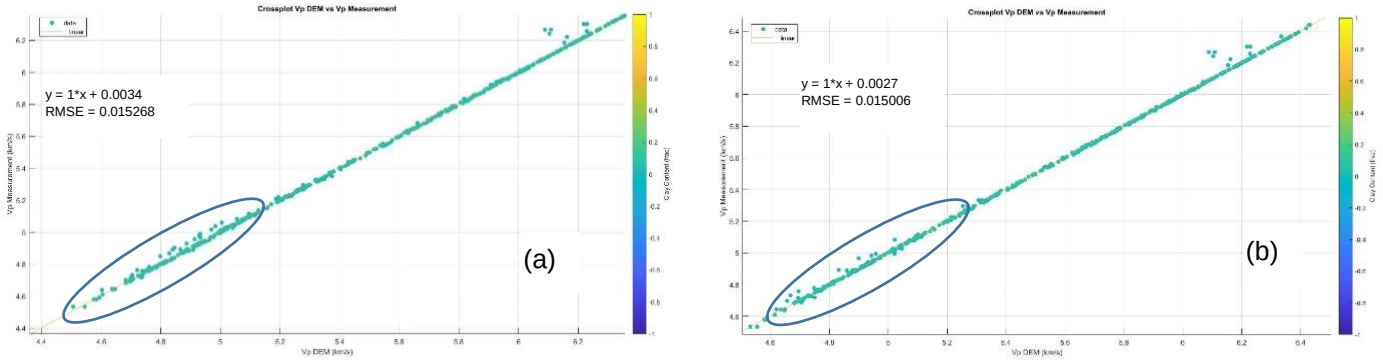

Figure 8. Cross plot between the value of V_p from the model and the measured value of V_p (a) before and (b) after optimization in RZ-09.

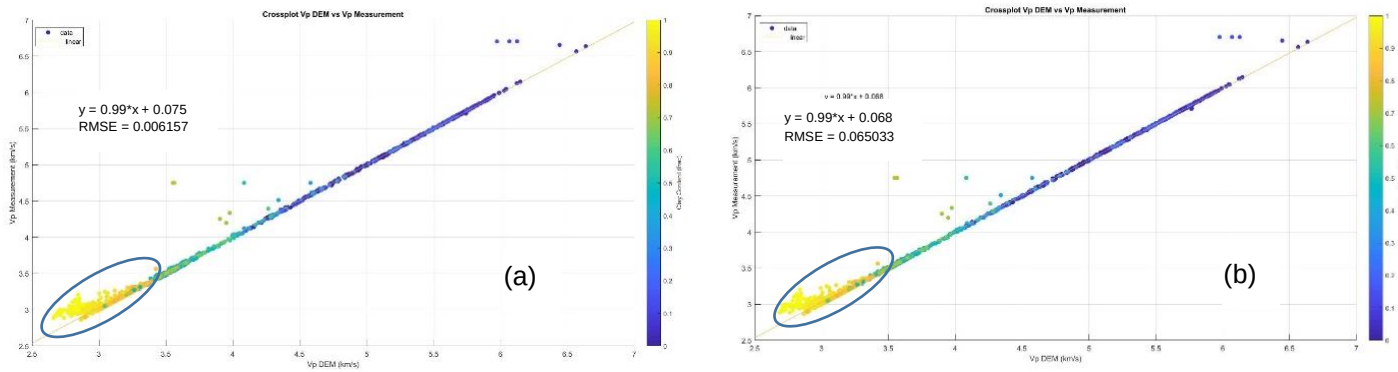

Figure 9. Cross plot between the value of V_p from the model and the measured value of V_p (a) before and (b) after optimization in RZ-35.

In RZ-09 the quadratic correlation coefficient is less than the linear one. This might be caused by the data scatter in RZ-09. In this case we conclude that there is some quartz mineral in the formation causing the linear correlation to be higher than the quadratic one, in line with the empiric V_p - V_s formula.[4]

4. Conclusion

Optimization of the rock physics modelling package DEM4 using fluid parameters obtained from the Adaptive Batzle-Wang method was successfully performed for the three wells RZ-14, RZ-09 and RZ-35. The value of the RMS error in the cross plot of the measured values of V_p against the values of V_p predicted by the model

can be minimized for each well, generating a rock model which closely approximates the actual conditions in the "R" field.

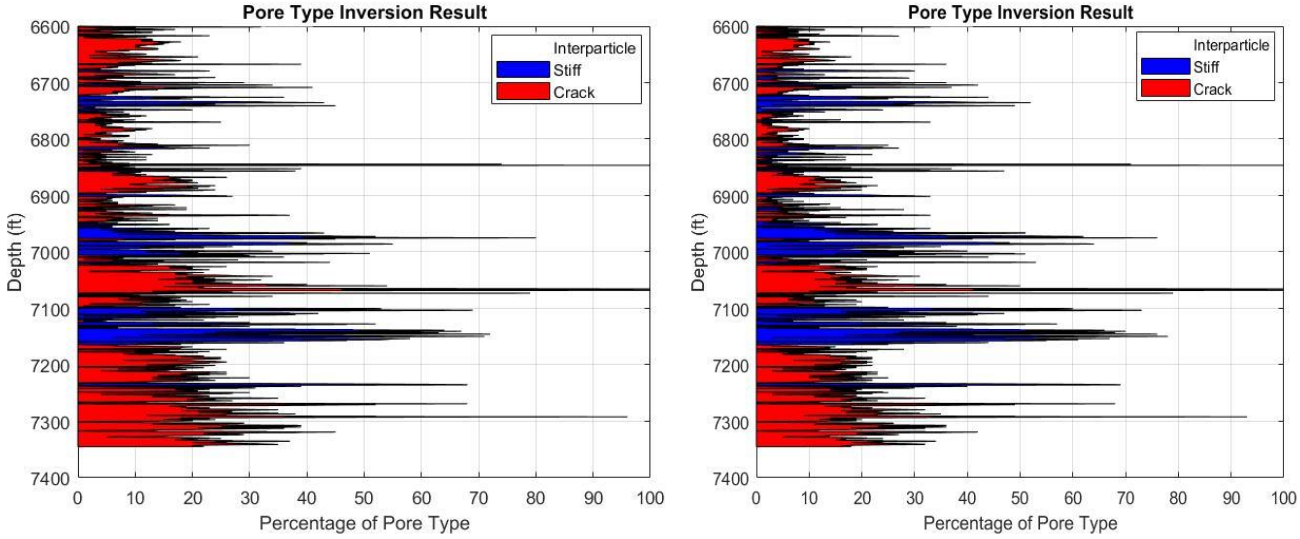

Figure 10. Pore Type Inversion before (left) and after (right) optimization in RZ-14.

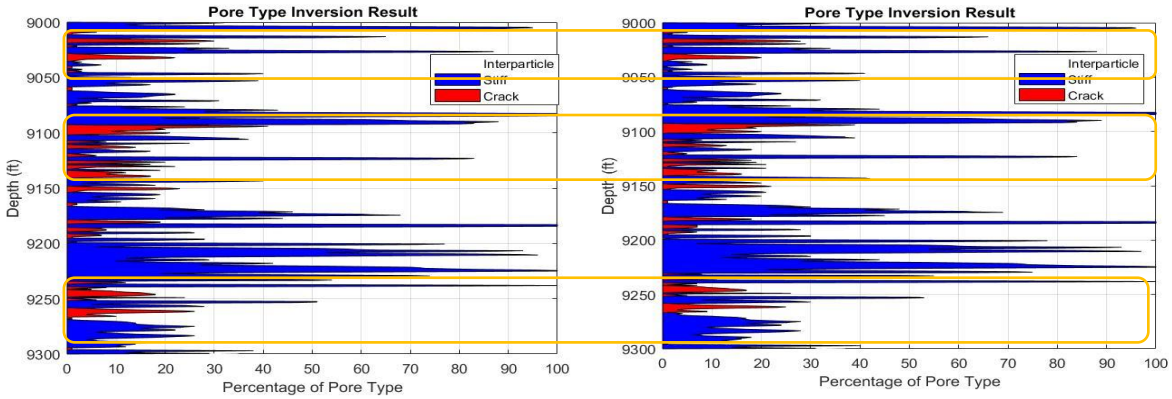

Figure 11. Pore Type Inversion before (left) and after (right) optimization in RZ-09.

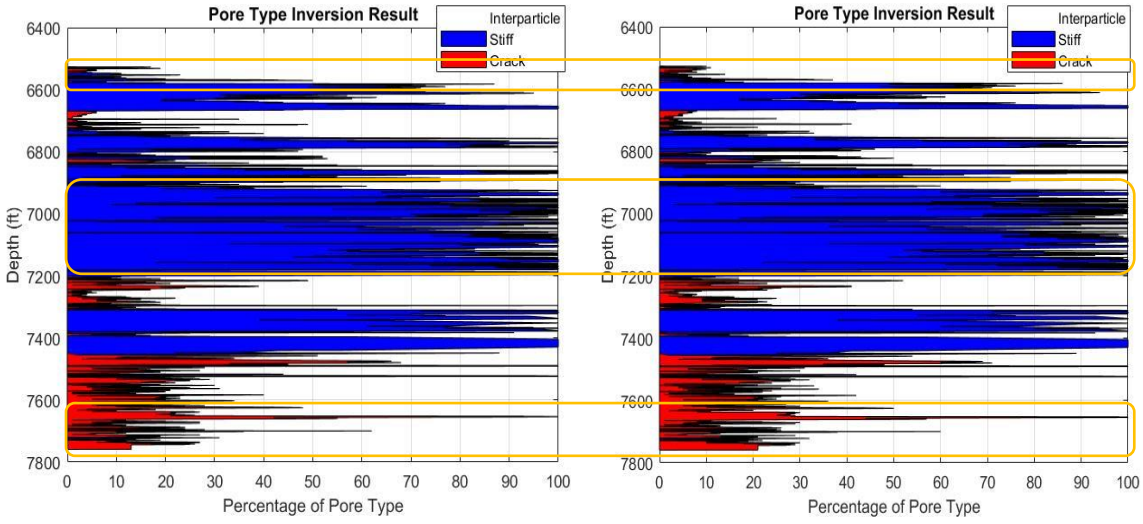

Figure 12. Pore Type Inversion before (left) and after (right) optimization in RZ-35.

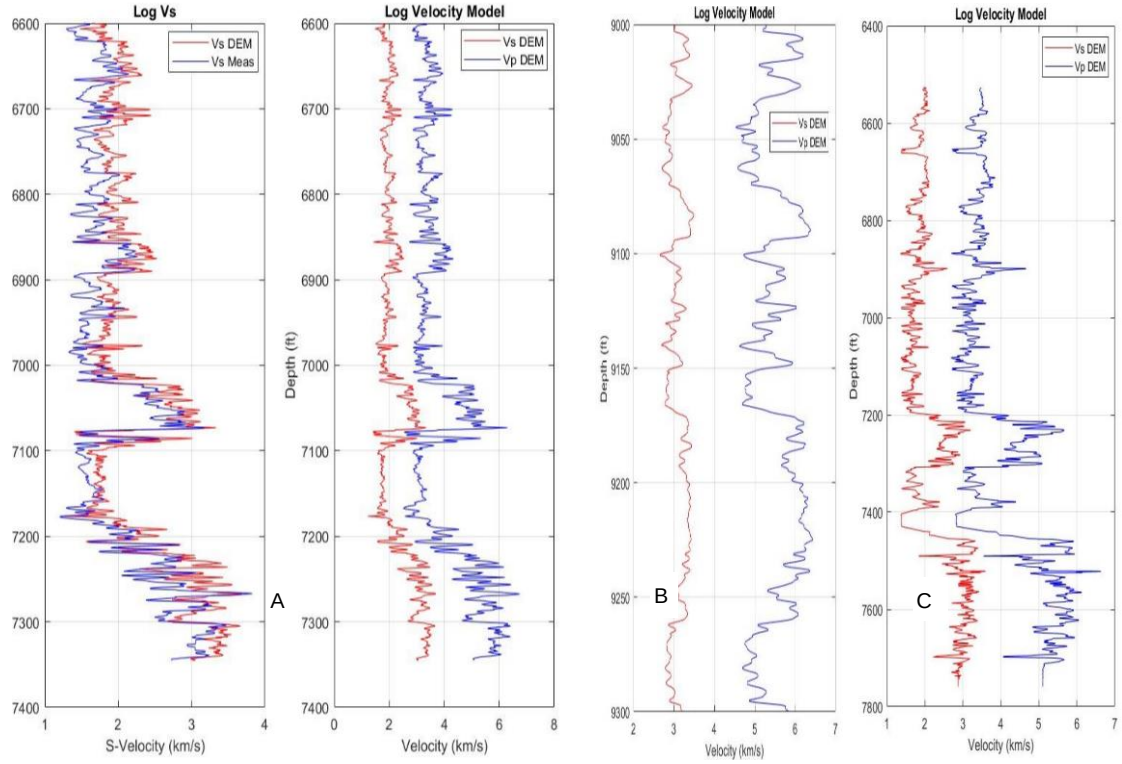

Figure 13. Optimized V_p and V_s log results in each well: (A) RZ-14, (B) RZ-09 and (C) RZ-35.

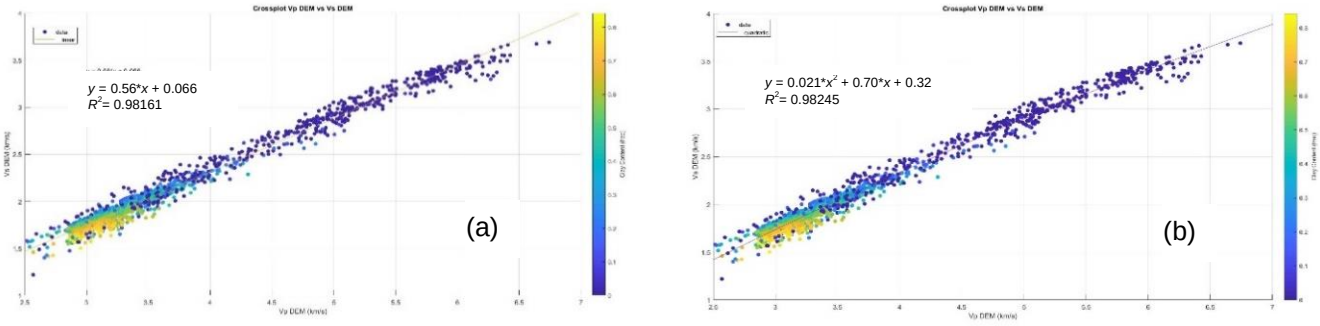

Figure 14. Cross plot between the values of V_p and V_s predicted by the model after optimization in RZ-14 using the (a) linear and (b) quadratic approach.

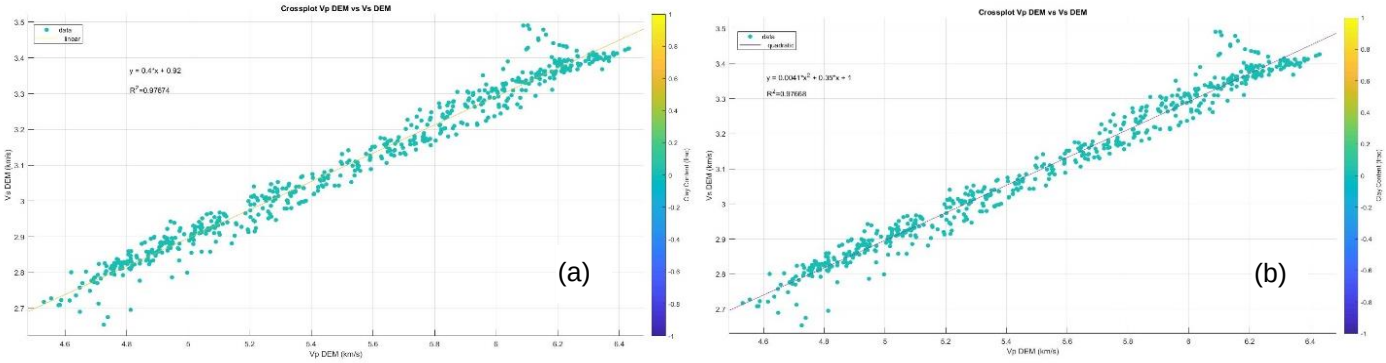

Figure 15. Cross plot between the values of V_p and V_s predicted by the model after optimization in RZ-09 using the (a) linear and (b) quadratic approach.

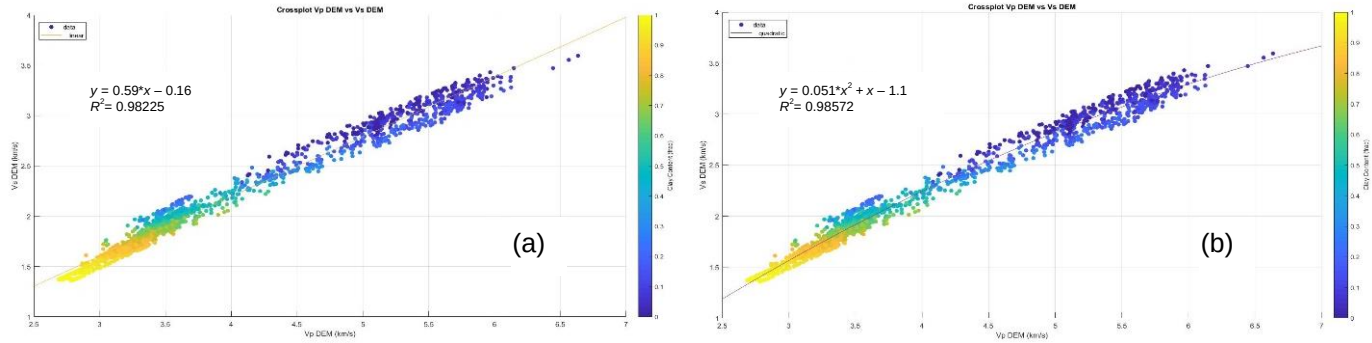

Figure 16. Cross plot between the values of V_p and V_s predicted by the model after optimization in RZ-35 using the (a) linear and (b) quadratic approach.

Acknowledgements

We would like to thank JOB–PERTAMINA Petrochina East Java for its permission to publish this data, as well as DRPM Universitas Indonesia for its financial support through the 2017 PITTA grant No. 663/UN2.R3.1/HKP.05.00/2017.

References

[1] M. S. Rosid, S. D. Wahyuni and M. W. Haidar, Carbonate Reservoir Characterization with Pore Type Inversion Using Differential Effective Medium (DEM) Model at "X" Field, East Java. *AIP Conference Proceedings*, **2017**, 1862, 030179 (2017); doi: 10.1063/1.4991283.

[2] Y. N. Candikia, M. S. Rosid and M. W. Haidar, Comparative Study between Kuster-Toksoz and Differential Effective Medium (DEM) Method for Determining Pore Type in Carbonate Reservoir. *AIP Conference Proceedings*, **2017**, 1862, 030185 (2017); doi: 10.1063/1.499128.

[3] G. Mavko, T. Mukerji, and J. Dvorkin, The Rock Physics Handbook: Tools for Seismic Analysis in Porous Media, **1998**, Cambridge University Press.

[4] J. P. Castagna, M. L. Batzle, and T. K. Kan, Rock Physics: The Link between Rock Properties and AVO Response. In: Offset- Dependent Reflectivity: Theory and Practice of AVO Analysis (eds. J. P. Castagna and M. Backus), **1993**, Investigation in Geophysics, SEG.

Characterization of a Reservoir Fluid Based on an Analysis of Intrinsic Properties Using the Adaptive Batzle-Wang Method in Field "M"

M. Syamsu Rosid[1], Muhammad Iksan[1], Reza Wardhana[1], and M. Wahdanadi Haidar[2]*

[1]Geophysics, FMIPA Universitas Indonesia, Depok 16424, Indonesia
[2]JOB Pertamina Petrochina East Java, Menara Kuningan Lt. 18 & 20, Jakarta 12940, Indonesia

**corresponding author email: syamsu.rosid@ui.ac.id*

Abstract

The physical properties and phases of a fluid under reservoir conditions are different from those under surface conditions. The value of a fluid property may change as a result of changes in pressure and temperature. An analysis of the intrinsic properties of fluids is carried out to obtain a fluid model that corresponds to fluid conditions in a reservoir. This study uses the Adaptive Batzle-Wang model, which combines thermodynamic relationships, empirical data trends, and experimental fluid data from the laboratory to estimate the effects of pressure and temperature on fluid properties. The Adaptive Batzle-Wang method is used because the usual Batzle-Wang method is less suitable for describing the physical properties of a fluid under the conditions in the field studied here. The Batzle-Wang fluid model therefore needs to be modified to obtain a fluid model that adjusts to the fluid conditions in each study area. In this paper, the Adaptive Batzle-Wang model is used to model three types of fluid i.e. oil, gas, and water. By making use of data on the intrinsic fluid properties such as the specific gravity of the gases (G), the Gas-Oil Ratio (GOR), the Oil FVF (B_o), the API values, the Salinity, and the Fluid Density obtained from laboratory experiments, the Batzle-Wang fluid model is converted into the Adaptive Batzle-Wang model by adding equations for the intrinsic fluid properties under the pressure and temperature conditions in the field reservoir. The results obtained are the values of the bulk modulus (K), the density (ρ), and the P-wave velocity (V_p) of the fluid under reservoir conditions. The correlation coefficient of the Adaptive Batzle-Wang model with the fluid data from the laboratory experiments is 0.95. The model is well able to calculate the fluid properties corresponding to the conditions in this field reservoir. The model also generates a unique value for the fluid properties in each study area. So, it can adjust to the pressure and temperature conditions of the field reservoir under study. The Adaptive Batzle-Wang method can therefore be applied to fields for which laboratory fluid data is available, especially fields with a high reservoir pressure and temperature. The results of the fluid modeling can then be used for rock physics and Fluid Replacement Model analysis.

Index Terms: fluid analysis, Adaptive Batzle-Wang, reservoir condition, fluid physical properties, fluid replacement model

1. Introduction

One main purpose of geophysical exploration is to describe the subsurface structure. One of the most commonly used methods is seismic prospecting, but this method has a poor resolution when estimating fluid properties in a reservoir, so that more accurate and reliable data is needed to describe the subsurface conditions. Downhole or well log data is often used to validate the seismic data. But in connecting the two methods it is necessary to use information from rock physics. Rock physics modeling can characterize the three main components of a reservoir: the rock, the pores, and the fluid that fills those pores. The fluids beneath the surface have different physical properties from those on

the surface due to the influence of the varying pressures and temperatures. However, the characterization of the fluid in a reservoir is often oversimplified in geophysical exploration, given that the fluid in the rock pores greatly affects the elastic properties inferred from the seismic data, so that more analysis is needed. One of the models that characterizes the fluid properties is the Batzle-Wang fluid model,[1] which combines thermodynamic theory, empirical data trends, and laboratory fluid data to estimate the effects of the fluid pressure and temperature. The Batzle-Wang method can be used to perform calculations with three types of fluids, namely hydrocarbon gas, oil and brine. The properties of each fluid are calculated using prior information. The approach used is based on equations obtained from an empirical formulation of the data extracted from the field. The results from the Batzle-Wang method are very useful for improving the accuracy of the Rock Physics model of the reservoir. The principal seismic properties characterizing a reservoir are the primary wave velocity (V_p) and density (ρ), which can be associated with the elastic modulus parameters. The elastic modulus of the fluid will also influence the characteristics of the reservoir, so the elastic properties of the fluid are calculated using the Batzle-Wang method. The Batzle-Wang model can be used to predict the fluid properties under the influence of varying pressure and temperature, but it is still less suitable for matching the properties to the reservoir conditions in the field under study. So we need to modify it to obtain a more accurate model. In this study we want to generate an empirical equation characterizing the fluid that can match the conditions in the subsurface reservoir in the "M" field. The method used in this study to identify the fluid properties by combining the empirical Batzle-Wang equations with the fluid analysis data from the laboratory is called the Adaptive Batzle-Wang fluid model. In general, the measured fluid properties such as the density (ρ), API, GOR (R_g), specific gravity (G), and Salinity (S) can be used to produce models of the density, the primary wave velocities and the fluid bulk modulus corresponding to the subsurface conditions. The data used as input for the Adaptive Batzle-Wang model comes from fluid sampling analysis in the laboratory, and is shown in ***Table 1***.

Table 1. Fluid analysis data from laboratory.

Data	Field	
	M-1	M-2
Specific Gas Gravity	√	√
API Degree	√	√
Gas-Oil Ratio	√	√
Oil volume Factor	√	√
Density of fluid	√	√

This study was conducted using data from fields M-1 and M-2, where the parameters studied include the Specific gravity of the Gas (G), the API value of the crude oil, the Gas-Oil Ratio (R_g), the Oil FVF (B_o), and the Density (ρ) of the fluid. By using the above data, we want to construct a fluid model that can match the fluid properties in each of the two fields, which have different pressure and temperature conditions. The study was conducted in two different fields, M-1 and M-2, so as to demonstrate the applicability of the Adaptive Batzle-Wang model. This in turn can be used to improve the accuracy of fluid replacement analysis, or equivalently the Fluid Replacement Model (FRM) method, which aims to identify and quantify reservoir fluids.[2] Rock physics modeling results are also used as validators to improve the accuracy of the Adaptive Batzle-Wang model.

2. Methodology

2.1 The Batzle-Wang method

The following summary of this model is taken from the original paper by Batzle and Wang.[1] The model combines thermodynamic theory and the empirical trends in the available data to predict the effects of pressure, temperature, and composition on the seismic properties of the fluid. Batzle and Wang examined the properties of gases, oils, and brine, the three main types of fluids found in almost all reservoirs. The fluid properties predicted include the bulk density and modulus (so speed is included) as functions of the fluid temperature and pressure, when the fluid composition is known or can be estimated. The

development of the complete fluid model is discussed in the original paper.[1] A brief summary of the fluid model, including the assumptions made and the equations used, will be discussed here. The model described here incorporates Gas, Live Oil, and Brine. When applying the Batzle-Wang model, it is assumed that at each point below the bubble point, the gas has the same properties/composition as the gas as a whole in the surface conditions. This means that there is no variation in the composition of the gas encountered during production. When applying the model, it is also assumed both that the oil left as a fluid after the gas is released (under the bubble point) has the same composition as the original Live Oil, and that the fluid is saturated with as much gas as possible in the conditions.

2.1.1 Elastic parameters of the hydrocarbon gas

The empirical equations used by Batzle and Wang to characterize the gas are derived from Thomas *et al.*[3] The relevant gas parameters are the Specific Gravity of the Gas (G), the Elastic Bulk Modulus of Gas (K_g) and the Gas Density (ρ_g). The elastic parameters can be calculated from the equation:

$$K_g = \frac{P}{\left(1 - \frac{P_{pr}}{Z}\frac{\partial Z}{\partial P_{pr}}\right)_T}\gamma_0 (1000)^{-1} \quad (1)$$

The value of the gas bulk modulus (K_g) is also influenced by the ratio of the heat capacity at constant pressure to the heat capacity at constant volume (γ_0),

$$\gamma_0 = 0.85 + \frac{5.6}{(P_{pr}+2)} + \frac{27.1}{(P_{pr}+3.5)^2} - 8.7\exp\left[-0.65(P_{pr}+1)\right] \quad (2)$$

where P is the pressure in GPa. If the data is quoted in Psi then a hydrostatic correction of 14.37 Psi must be added, and the pressure then converted into GPa. The pressure is calculated from the value of P_{pr} (the pseudoreduced Pressure), which is obtained from the value of Ppc (the pseudocritical Pressure), according to the following formulas from Katz *et al.*[4] and Thomas *et al.*:[3]

$$P_{pr} = \frac{P}{P_{pc}} \quad (3)$$

$$P_{pc} = 4.892 - 0.4048G \quad (4)$$

$$\rho_g = \frac{28.8GP}{ZRT_a} \quad (5)$$

where R is the universal gas constant (8.3145 m^3 Pa/(mol-K)) and T_a is the temperature in Kelvins. Most temperature measurements in the field are quoted in Fahrenheit and must be converted to Celsius and then to Kelvin for Hydrocarbon Gas modeling.[3,4] The relevant formulas are:

$$T_{pr} = \frac{T_a}{T_{pc}} \quad (6)$$

$$T_a = T(^oC) + 273.15 \quad (7)$$

$$T_{pc} = 94.72 + 170.75G \quad (8)$$

where T_{pr} is the pseudoreduced Temperature and T_{pc} is the pseudocritical Temperature. Calculation of the gas bulk modulus (K_g) and Gas Density (ρ_g) is also influenced by the compressibility factor (z), which is given by the following equations from Thomas *et al.*:[3]

$$z = \left[0.03 + 0.0052\left(3.5 - T_{pr}\right)^3\right]P_{pr} + \left(0.642T_{pr} - 0.007T_{pr}^4 - 0.52\right) + E \quad (9)$$

$$E = 0.109\left(3.85 - T_{pr}\right)^2 \exp\left\{-\left[0.45 + 8\left(0.56 - \frac{1}{T_{pr}}\right)^2\right]\frac{P_{pr}^{1.2}}{T_{pr}}\right\} \quad (10)$$

$$\frac{\partial z}{\partial P_{pr}} = A + 0.1308\left(3.85 - T_{pr}\right)^2 \exp\left(BP_{pr}^{1.2}\right)BP_{pr}^{0.2} \quad (11)$$

$$A = 0.03 + 0.00527\left(3.5T_{pr}\right)^3 \tag{12}$$

$$B = \left(\frac{-1}{T_{pr}}\right)\left(0.45 + 8\left(0.56 - \frac{1}{T_{pr}}\right)^2\right) \tag{13}$$

2.1.2 Elastic parameters of the live oil

The Live Oil is a gas-saturated oil hydrocarbon and therefore the parameters affecting the elastic properties of the Live Oil include the Specific Gas gravity (G), the API value of the crude oil, the Gas-Oil Ratio (R_g), the Oil FVF (B_o), and the Density (ρ) of the Live Oil. The Live Oil Density (ρ) can be calculated from a formula due to Dodson and Standing:[5]

$$\rho_\ell = \left[\frac{\rho_{pl}}{0.972 + \left(3.81\times10^{-4}\right)\left(T + 17.78\right)^{1.175}}\right] \tag{14}$$

The value of the Density (ρ) of the Live Oil in g/cm^3 is obtained by calculating ρ_{pl} (the density at the given pressure) and ρ_{gl} (the density due to the influence of saturated gas) through the following equations, due to McCain:[6]

$$\rho_{pl} = \rho_{gl} + \left(0.00277P - \left(1.71\times10^{-7}\right)P^3\right)\left(\rho_{gl} - 1.15\right)^2 + \left(3.49\times10^{-4}\right)P \tag{15}$$

$$\rho_{gl} = \frac{\left(\rho_0 + 0.0012GR_g\right)}{B_{ol}} \tag{16}$$

The Density (ρ) of the Live Oil is also influenced by both the Gas-Oil Ratio (R_g) and the Oil Formation Volume Factor (B_o), which in turn are affected by the API values of the Live Oil:[7]

$$R_G = 0.02122G\left[P\exp\left(\frac{4.072}{\rho_0}\right) - 0.00377T\right]^{1.205} \tag{17}$$

$$B_{ol} = 0.972 + 0.0003812\left[2.4955R_g\sqrt{\frac{G}{\rho_0}} + T + 17.778\right]^{1.175} \tag{18}$$

$$\rho_0 = \frac{141.5}{API + 131.5} \tag{19}$$

Wang[8] and Wang *et al.*[9] have shown that the ultrasonic velocity of a variety of oils decreases rapidly with density (increasing API). The P-wave velocity of the Live Oil (V_l) calculated in m/s is also influenced by the GOR (R_g) and the Oil FVF (B_o), through the pseudodensity ρ_{dl} generated by the presence of dissolved gas in the Live Oil. The equations used are as follows:

$$V_l = 2096\sqrt{\frac{\rho_{dl}}{2.6 - \rho_{dl}}} - 3.7T + 4.64P + 0.0115\left[4.12\sqrt{\frac{1.08}{\rho_{dl}} - 1} - 1\right]TP \tag{20}$$

$$\rho_{dl} = \frac{\rho_0}{B_{ol}}\left(1 + 0.001R_g\right)^{-1} \tag{21}$$

The Live Oil Bulk Modulus (K_l) in units of GPa is calculated from the density (ρ_l) and velocity of the Live Oil (V_l) through the equation:

$$K_l = \left(V_l^2 \rho_l\right) 1000^{-1} \tag{22}$$

2.1.3 Elastic parameters of the brine

The main parameter affecting the brine is its salinity (S). In the Batzle-Wang brine model, the salinity used is the weight of the NaCl fraction (in ppm/1,000,000). So the salinity will have an effect on the values of the brine density (ρ_b) and the brine velocity (V_b). The relevant equations are due to Zarembo and Fedorov[10] and Potter and Brown,[11] and are as follows:

$$\rho_w = 1 + \left(10^{-6}\left(-80T - 3.3T^2 + 0.00175T^3 + 489P - 2TP + 0.016T^2P - \left(1.3\times10^{-5}\right)T^3P - 0.333P^2 - 0.002TP^2\right)\right) \tag{23}$$

$$\rho_b = \rho_w + S\left\{0.668 + 0.44S + \left(1\times10^{-6}\right)\left[300P - 2400PS + T\left(80 + 3T - 3300S - 13P + 47PS\right)\right]\right\} \tag{24}$$

where ρ_w is the fresh water density in g/cm^3, whose value is influenced by the pressure and temperature in the reservoir. The density of the brine (ρ_b) is calculated on the basis of the fresh water density (ρ_w) with corrections made for the effects of salinity (S). Following Wilson,[12] the primary wave velocity in the fresh water (V_w) in m/s is calculated from field measurement data and the coefficients W_{ij} obtained from ***Table 2***. The relevant equation is:

$$V_w = \sum_{i=0}^{4}\sum_{j=0}^{3} W_{ij} T^i P^j \tag{25}$$

The primary wave velocity of the brine (V_b) is taken from Chen *et al.*,[12] and is calculated by combining the fresh water wave velocity (V_w) with the Salinity (S).

$$\begin{aligned} V_b = V_w + S\left(1170 - 9.6T + 0.055T^2 - \left(8.5\times10^{-5}\right)T^3 + 2.6P - 0.0029TP - 0.0476P^2\right) + \\ S^{1.5}\left(780 - 10P + 0.16P^2\right) - 820S^2 \end{aligned} \tag{26}$$

So, on using the equations for the brine density (ρ_b) and brine velocity (V_b), the value of the brine bulk modulus (K_b) without gas saturation in GPa is

$$K_b = \left(V_b^2 \rho_b\right) 1000^{-1} \tag{27}$$

2.2 The Adaptive Batzle-Wang Method

The Adaptive Batzle-Wang model uses the Batzle-Wang empirical equations and fluid parameters from the laboratory, namely the bulk modulus (K), density (ρ), and P-wave velocity (V_p), to characterize the fluid. The Adaptive Batzle-Wang method generates models for the Gas, Live Oil, and Brine fluid fractions. Of these, the Brine model in the Adaptive Batzle-Wang method is the same as in the Batzle-Wang fluid model because the effects of Salinity in each field are almost the same because the salt composition tends not to differ between fields, unlike the hydrocarbon gas and oil compositions, which are highly variable. The three elastic parameters for the fluid mentioned above are influenced by the API, the Specific Gravity of the Gas (G), the Gas-Oil Ratio (R_g), the Oil FVF (B_o), the Salinity (S), and the Density of the fluid (ρ), and the parameters will change as the pressure and temperature vary at each level below the surface. The output of the method is the values of the bulk modulus (K), density (ρ), and primary wave velocity (V_p) in the fluid, calculated using the pressure and temperature in the reservoir as input together with some rock physics analysis. The model uses the Batzle-Wang fluid mixing results found by applying the Woods Relation to the rock matrix. The model utilizes the laboratory data and the empirical Batzle-Wang equations to obtain a model that is more appropriate for the fluid conditions in the reservoir under study. Due

to the effects of changes in the pressure and temperature the values of the Specific Gravity of the Gas (G), the Gas-Oil Ratio (R_g), the oil FVF (B_o), and the fluid density (ρ_{fl}) can vary between depth levels in each field, so the fluid parameters generated by the basic Batzle-Wang model might not be appropriate for the field conditions.

Table 2. Coefficients used for calculating the primary wave velocity in water provided by Milero *et al.*[13] and Chen *et al.*[12]

W_{00} =	1402.85	W_{02} =	3.437×10^{-3}
W_{10} =	4.871	W_{12} =	1.738×10^{-4}
W_{20} =	-0.04783	W_{22} =	-2.135×10^{-6}
W_{30} =	1.487×10^{-4}	W_{32} =	-1.455×10^{-8}
W_{40} =	-2.197×10^{-7}	W_{42} =	5.230×10^{-11}
W_{01} =	1.524	W_{03} =	-1.197×10^{-5}
W_{11} =	-0.0111	W_{13} =	-1.628×10^{-6}
W_{21} =	2.747×10^{-4}	W_{23} =	1.237×10^{-8}
W_{31} =	-6.503×10^{-7}	W_{33} =	1.327×10^{-10}
W_{41} =	7.987×10^{-10}	W_{43} =	-4.614×10^{-13}

2.3 The Woods equation

The output from the Adaptive Batzle-Wang method, namely the values of the Bulk modulus (K) and Density (ρ) for each fluid, is then used to model the fluid mixture. A relation often used in fluid mixing analysis is the Woods equation, here taken from Mavko *et. al.*:[14]

$$\frac{1}{K_{FL}} = \frac{S_{Water}}{K_{Water}} + \frac{S_{Oil}}{K_{Oil}} + \frac{S_{Gas}}{K_{Gas}} \qquad (28)$$

where S_{water} is the water saturation, S_{oil} is the oil saturation, S_{gas} is the gas saturation, K_{water} is the bulk modulus of the water, K_{oil} is the bulk modulus of the oil, K_{gas} is the bulk modulus of the gas, and K_{fl} is the bulk modulus of the fluid mixture.

$$\rho_{fl} = \rho_w S_w + \rho_{Hyc}(1 - S_w) \qquad (29)$$

To apply the Fluid Replacement Model (FRM) the density of the mixed fluid (ρ_{fl}), obtained by incorporating the fluid saturation, is also required at each depth.

2.4 The Voight-Reuss-Hill Method

To demonstrate that the Adaptive Batzle-Wang method calculates the elastic parameters of the fluid with improved accuracy, rock physics modeling must be performed to test the accuracy of the elastic parameters. It is therefore necessary to model the minerals in the rock matrix in conjunction with the model for the fluid saturations provided by the Woods relation. The equation for the elastic modulus of the rock matrix generated by the VRH method is as follows:[14]

Voight Method: $$M_V = \sum_{i-n}^{N} f_i . M_i \qquad (30)$$

Reuss Method: $$\frac{1}{M_R} = \sum_{i-1}^{N} \frac{f_i}{M_i} \qquad (31)$$

Voight-Reuss-Hill Method:

$$M_{VRH} = \frac{M_V + M_R}{2} \qquad (32)$$

where the M_V is the Voight elastic modulus, M_R is the Reuss elastic modulus, M_{VRH} is the Voight-Reuss-Hill elastic modulus, f_i is the fraction of mineral i and M_i is the elastic modulus of mineral i.

2.5 Rock physics analysis

To test the accuracy of the fluid model, we apply rock physics analysis using the Differential Effective Medium (DEM) method to validate the elastic parameters. The DEM method models a two-phase composite by incrementally adding a small number of pores to the matrix. In the DEM method, the values of the effective moduli depend on the construction path taken to reach the final composite. The DEM method works by adding inclusions to the background model. The model is continuously changing as the inclusions are added.[14] The results of the fluid mixing from the Woods equation and the rock matrix modeling from the VRH method are used to calculate the primary wave velocity (V_p) in the saturated rock. It is therefore possible to check if the V_p value generated by the model is close to the measured V_p value. By this means, it can be determined if the saturated V_p value from the

Adaptive Batzle-Wang model is more accurate than the value from other models. The most accurate model is that which has the smallest root-mean-square-error (RMSE) after regression of the predicted and measured V_p values. In this paper, we compare the RMSE values generated by the rock physics DEM method for the Batzle-Wang fluid model and the modified model, which is the Adaptive Batzle-Wang fluid model.

2.6 Fluid Replacement Model

This study combines the Batzle-Wang fluid model and experimental fluid data from the laboratory to produce the Adaptive Batzle-Wang fluid model. In the process, the Adaptive Batzle-Wang model generates values of the Bulk Modulus (K), and Density (ρ) for each type of fluid, which are then mixed using the Woods equation and used as inputs for the rock physics analysis to obtain the primary wave velocity in the saturated rock (Vp), which is calculated from the following equation due to Han and Batzle:[2]

$$V_p = \sqrt{\frac{K + \frac{4}{3}\mu}{\rho}} \tag{33}$$

The Adaptive Batzle-Wang method can then be applied to generate a Fluid Replacement Model (FRM) using the Gassmann equation,[15] shown below:

$$K_{sat} = K_{dry} + \frac{\left(1 - \frac{K_{dry}}{K_m}\right)^2}{\frac{\phi}{K_f} + \frac{(1-\phi)}{K_m} - \frac{K_{dry}}{K_m^2}} \tag{34}$$

where K_{sat} is the bulk modulus of the fluid-saturated rock, K_{m} is the bulk modulus of the minerals, K_{f} is the bulk modulus of the pore fluid, K_{dry} is the bulk modulus of the rock frame, and ϕ is the porosity.

3. Results and Discussion

The values of the elastic parameters of the fluid calculated from the usual Batzle-Wang and the Adaptive Batzle-Wang models in the two different fields are shown in ***Table 3***.

Table 3 shows that the results from the Adaptive Batzle-Wang model are better than those from the Batzle-Wang model. The calculated values of the Bulk Modulus (K), Density (ρ), and Slowness for Live Oil in Field M-1 (P = 2925 P_{sig}, T = 235 F, API = 40) and Field M-2 (P = 3850 P_{sig}, T = 291 F, API = 35.1) from the Adaptive Batzle-Wang model are closer to the measured laboratory values.

The calculated values from the Batzle-Wang model have a larger percentage error than those from the Adaptive Batzle-Wang model, as can be seen in ***Table 4*** and ***Table 5***. The advantages of the Adaptive Batzle-Wang method are due to the modification of the empirical Batzle-Wang equations produced by incorporating the laboratory fluid data. In addition, the pressure (P) and temperature (T) values used as inputs in the Adaptive Batzle-Wang model are changed to match the varying P and T states at each depth, according to the P and T input logs in ***Figure 1***.

The Pressure and Temperature inputs from ***Figure 1*** are then used in the Adaptive Batzle-Wang model to obtain elastic parameters corresponding to the fluid conditions in the two fields, according to the bulk modulus logs in ***Figure 2***.

From ***Figure 2*** it can be seen in the Live Oil log that the value of the bulk modulus is 517.056 MPa for field M-1 and 625,824 MPa for field M-2. The bulk modulus calculated from Fig. 2 is then used as an input for the rock physics model. To demonstrate that the Adaptive Batzle-Wang model produces more accurate fluid parameters than the Batzle-Wang model this study uses the pore Differential Effective Medium (DEM) inversion method, as explained in Section 5.

From ***Figure 3*** and ***Figure 4*** it can be seen that the root-mean-square-error (RMSE) between the measured V_p values and the V_p values calculated by applying the rock physics DEM method to the results from the Adaptive Batzle-Wang model is smaller than the RMSE between the measured values and the values calculated from the Batzle-Wang model. So it can be concluded that the fluid parameters are more accurately calculated

using the Adaptive Batzel-Wang model. In fact, in terms of percentage differences, the Adaptive Batzel-Wang model is 17.03% better than the Batzle-Wang model in the M-1 field and 5.82% better in the M-2 field. The Adaptive Batzle-Wang model and the rock physics DEM method can also be combined with the Gassmann equation to obtain a Fluid Replacement Model (FRM). The results of the FRM can be used to model V_p, V_s, and ρ. By applying the fluid replacement model, it is possible to assess the sensitivity of the Adaptive Batzel-Wang fluid model. This also demonstrates that the output of the Adaptive Batzle-Wang model generates an appropriate Fluid Replacement Model.

Table 3. Comparison of the calculated fluid parameters with the laboratory measurements.

Input		Parameter of Live Oil	BW	ABW	Lab
P =	2925 P_{sig}	Bulk Modulus (Mpa)	441.6765	517.056	516.327
T =	235 F	Density (g/cc)	0.6283	0.6181	0.6182
API =	40	Slowness (us/ft)	363.5451	333.252	333.512
P =	3850 P_{sig}	Bulk Modulus (Mpa)	399.5628	625.8242	625.405
T =	291 F	Density (g/cc)	0.6632	0.6953	0.6956
API =	35.1	Slowness (us/ft)	377.9277	321.2821	321.46

Table 4. Percentage differences between the Batzle-Wang and Adaptive Batzle-Wang model values and the measured laboratory values for field M-1.

Input		Parameter of Live Oil	Difference of BW (%)	Difference of ABW (%)
P =	2925 P_{sig}	Bulk Modulus (Mpa)	14.46	0.14
T =	235 F	Density (g/cc)	1.63	0.02
API =	40	Slowness (us/ft)	9.01	0.08

Table 5. Percentage differences between the Batzle-Wang and Adaptive Batzle-Wang model values and the measured laboratory values for field M-2.

Input		Parameter of Live Oil	Difference of BW (%)	Difference of ABW (%)
P =	3850 P_{sig}	Bulk Modulus (Mpa)	36.11	0.07
T =	291 F	Density (g/cc)	4.66	0.04
API =	35.1	Slowness (us/ft)	17.57	0.06

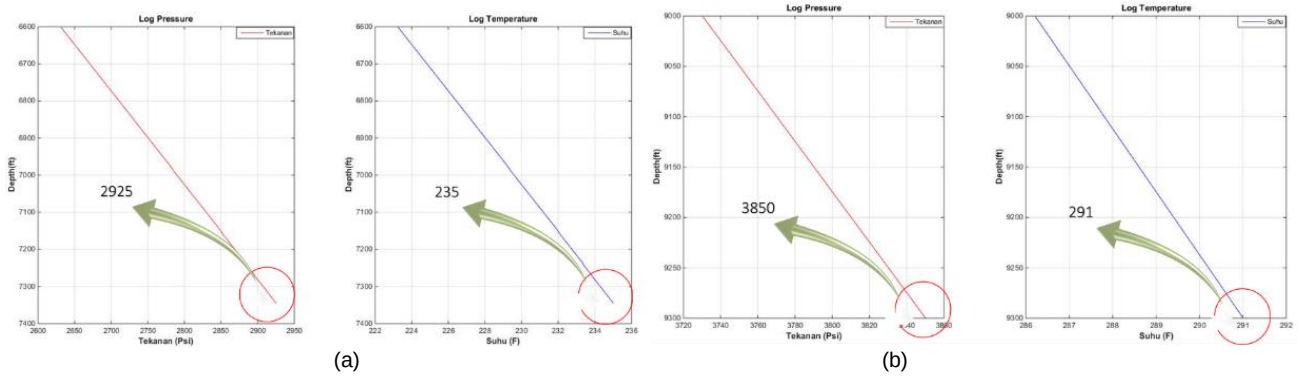

(a) (b)

Figure 1. Input Pressure and Temperature logs for field M-1 (a) and field M-2 (b) (*P*=2925 P_{sig}, *T*=235 F, API=40).

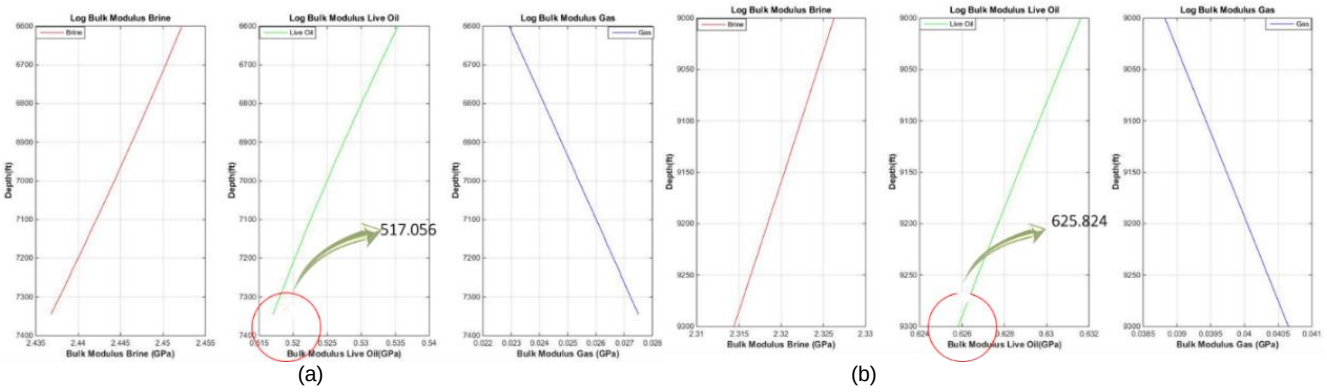

Figure 2. Bulk modulus Logs used in the Adapative Batzle-Wang model for field M-1 (a) and field M-2 (b).

From ***Figure 3*** and ***Figure 4*** it can be seen that the root-mean-square-error (RMSE) between the measured V_p values and the V_p values calculated by applying the rock physics DEM method to the results from the Adaptive Batzle-Wang model is smaller than the RMSE between the measured values and the values calculated from the Batzle-Wang model. So it can be concluded that the fluid parameters are more accurately calculated using the Adaptive Batzel-Wang model. In fact, in terms of percentage differences, the Adaptive Batzel-Wang model is 17.03% better than the Batzle-Wang model in the M-1 field and 5.82% better in the M-2 field. The Adaptive Batzle-Wang model and the rock physics DEM method can also be combined with the Gassmann equation to obtain a Fluid Replacement Model (FRM). The results of the FRM can be used to model V_p, V_s, and ρ. By applying the fluid replacement model, it is possible to assess the sensitivity of the Adaptive Batzel-Wang fluid model. This also demonstrates that the output of the Adaptive Batzle-Wang model generates an appropriate Fluid Replacement Model.

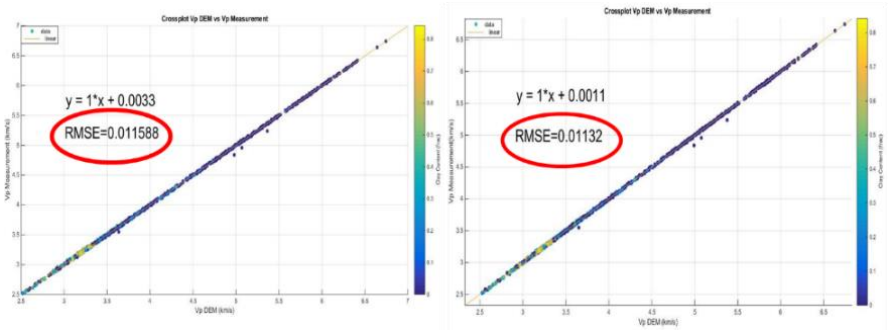

Figure 3. Results of the DEM method regression for the primary wave velocity (*V*p) values from (a) the Batzlel-Wang model (b) the Adaptive Batzle-Wang model in field M-1.

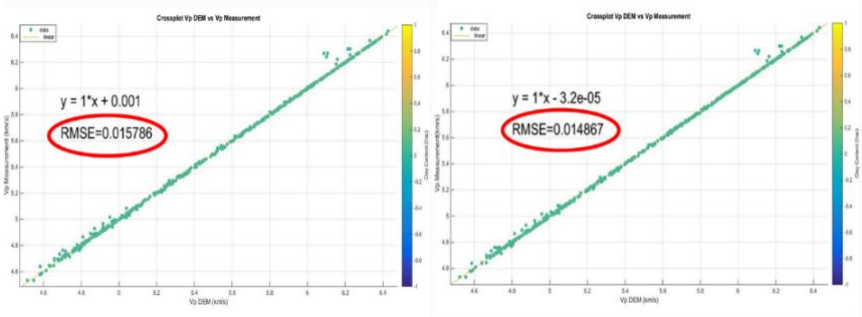

Figure 4. Results of the DEM method regression for the primary wave velocity (*V*p) values from (a) the Batzlel-Wang model (b) the Adaptive Batzle-Wang model in field M-2.

The results in ***Figure 5*** can be interpreted as showing that there are carbonate zones at depths of about 7000-7100 and 7200-7400 ft. This conclusion is reinforced by the very small clay volume log at these depths, and the logs also display a high density and low porosity there. The small values in the log of V_p (slowness in μs/ft) indicates that there is denser lithology here than elsewhere. This is due to the effect of the carbonates at these depths.

From ***Figure 6*** it can be seen that different water saturations correspond to shifted V_p curves in the two models. This shows that differences in the fluid content will affect the values of V_p.

Figure 7 shows that the log is of a clean carbonate formation. This can be seen from the log of clay volumes, which are zero. From ***Figure 7*** it can be conjectured that there is a stiff carbonate zone filled with fluid or cementation. In the zones with red and yellow markers fluid is suspected because the porosity in the zones is large and the density is small, and the small values in the V_p log confirm the presence of fluid. The zones with blue and black markers are suspected to be dolomitized stiff carbonate zones because of their decreased porosity and increased density, as well as the large values in the V_p log. The layers are suspected to be compact zones formed by diagenetic processes. Comparison of the DEM model with the measurements shows considerable differences in the carbonate zone because the secondary porosity in the DEM model adjusts more to the conditions of the pore type, while the V_p measurements from the FRM only take account of the total porosity in the formation.

The varying water saturations of 10%, 40%, and 100% indicate differences in the fluid content. In zones with red and yellow markers the fluid saturation is between 40% and 60%. The presence of hydrocarbons is supported by the porosity and density logs in ***Figure 7***, as there is a zone suspected of containing 60% hydrocarbons. Also, the zones with blue and black markers indicate that 100% water saturation best matches the in-situ saturation. It is suspected that water fills the formation and causes dolomitization, thus increasing the rock density. The results obtained will indicate whether the output of the Adaptive Batzle-Wang model is sensitive to the secondary porosity values from the DEM modeling.

4. Conclusions

The reservoir fluid can be characterized by the values of the bulk modulus, density, and primary wave velocity. These three parameters are heavily influenced by the pressure and temperature, and the intrinsic properties of each fluid also affect the results of the reservoir fluid modeling. The presence of fluid affects the rock physics, so the accuracy and suitability of the fluid model should be investigated more deeply. Modeling the fluid in the M-1 and M-2 fields by using the Batzle-Wang model modified by the inclusion of fluid data from the laboratory yields an improvement in the accuracy of the rock physics parameters compared with the values predicted in surface conditions. The Adaptive Batzle-Wang model therefore provides a more accurate description of the fluid. The model is applicable to reservoir fluids under a variety of field conditions, especially at high pressures and temperatures. This model can also be adapted easily to the conditions in the field by using fluid data from the field. Accurate fluid models are also very useful for the construction of fluid replacement models.

5. Additional Considerations

The results from the Adaptive Batzle-Wang model will be more convincing if more fluid data from laboratory measurements is available. The trends used in the empirical equations will then be more accurate, especially if data is available for each sample of gas, oil, and water. The method also requires data on the pressure and temperature in the area under study. A lack of such detailed data is the main challenge to extending the applicability of the method.

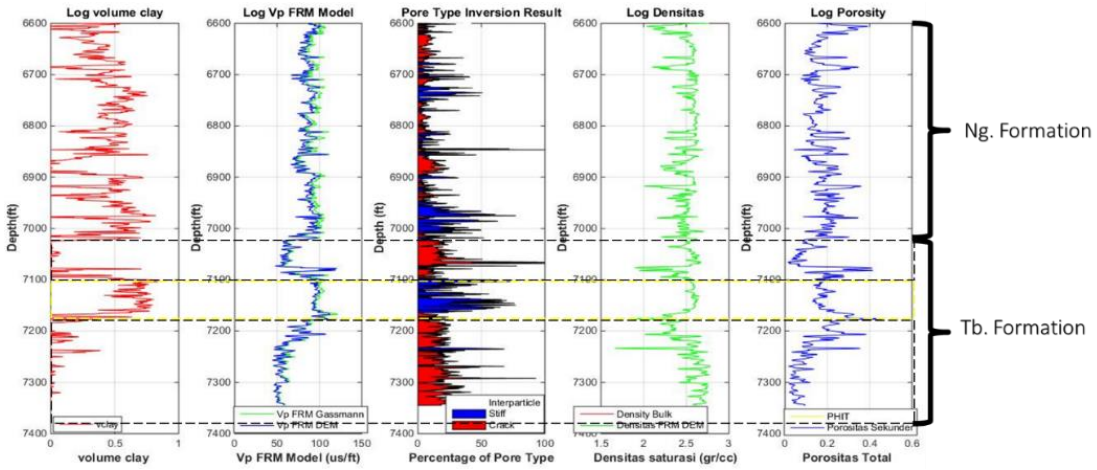

Figure 5. Values of V_p calculated using the Adaptive Batzle-Wang model and the FRM in field M-1.

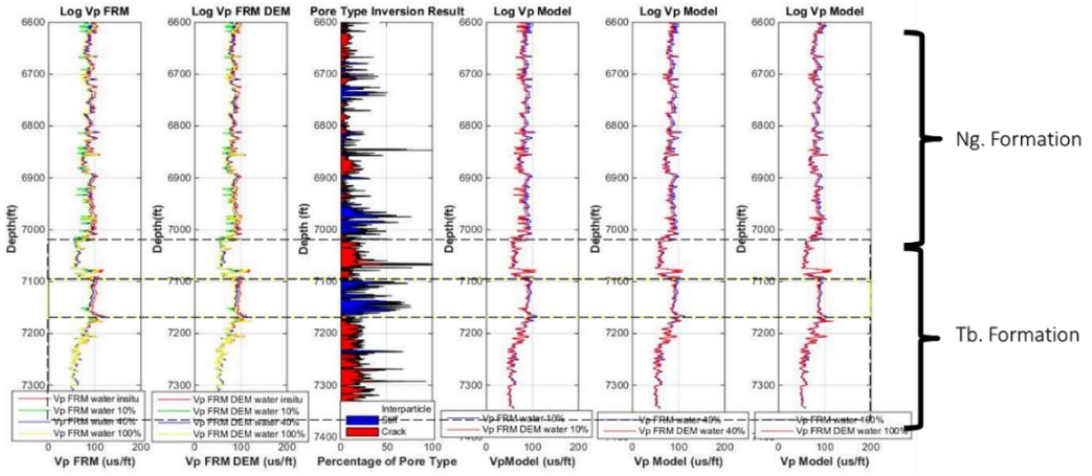

Figure 6. Comparison Logs of the values of the primary wave velocity V_p calculated using the Adaptive Batzle-Wang model, the FRM and the combined FRM/DEM model and the measured V_p values in field M-1.

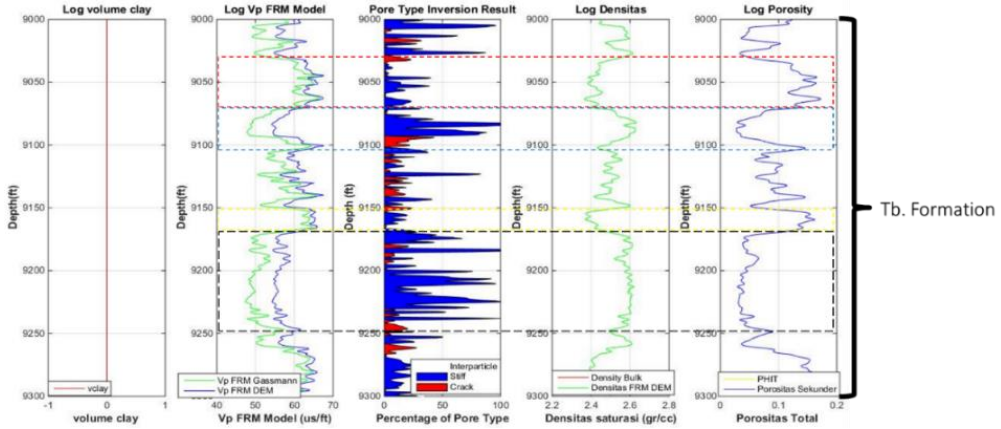

Figure 7. Values of V_p calculated using the Adaptive Batzle-Wang model and FRM in field M-2.

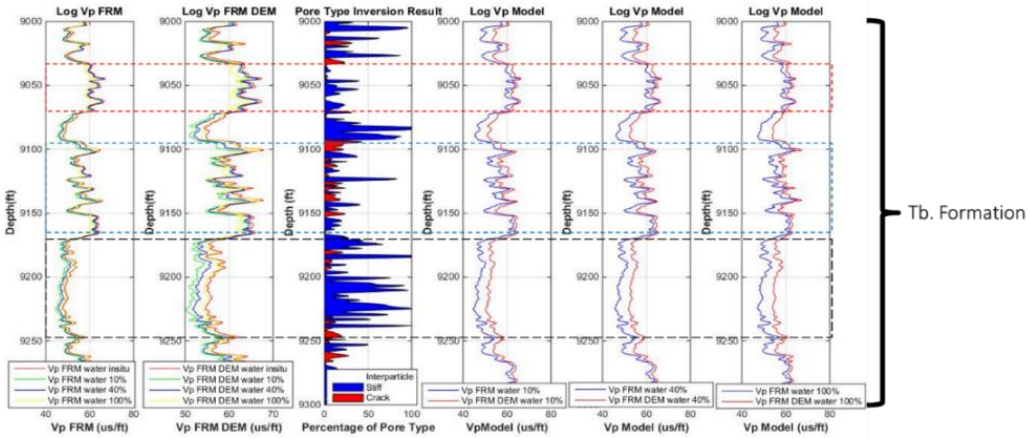

Figure 8. Comparison Logs of the values of the primary wave velocity *Vp* calculated using the Adaptive Batzle-Wang model, the FRM and the combined FRM/DEM model and the measured *Vp* values in field M-2.

Acknowledgements

We wish to express our thanks to JOB-Pertamina Petrochina East Java for its support in providing us with the data. Also our thanks go to DRPM Universitas Indonesia for its financial support through the 2017 PITTA grant No. 663/UN2.R3.1/HKP.05.00/2017.

References

[1] M. Batzle and Z. Wang, Seismic properties of pore fluids. *Geophysic*. **1992**, 57, 1396–1408.

[2] D. Han and M. L. Batzle, Gassmann's Equation and Fluid-saturation Effects on Seismic Velocities. *Geophysic*., **2004**, 69, 398-405.

[3] L. K. Thomas, R. W. Hankinson and K. A. Phillips, Determination of acoustic velocities for natural gas, *J. Petr. Tech*., **1970**, 22, 889-892.

[4] D. L. Katz, D. Cornell, J. A. Varv, R. Kobavashi, J. R. Elenbaas, F. H. Poettmann and C. F. Weinaug, Handbook of Natural Gas Engineering, **1959**, McGraw-Hill Book Co.

[5] C. R. Dodson, and M. B. Standing, Pressure-volume-temperature and solubility relations for natural-gas-water mixtures: in drilling and production practices, *Drilling and production practice*, **1944**.

[6] W. D. McCain, Properties of Petroleum Fluids, **1973**, Petroleum Pub. Co.

[7] M. B. Standing, Oil systems correlations, in: Petroleum production handbook (ed. T. C. Frick), **1962**, volume II, McGraw-Hill Book Co., part 19.

[8] Z. W. Wang, Wave velocities in hydrocarbons and hydrocarbon saturated rocks-with applications to EOR monitoring, **1988**, Ph.D. thesis, Stanford Univ.

[9] Z. Wang, A. Nur, and M. L. Batzle, Acoustic velocities in petroleum 011s, Sot. Petr. Eng. (SPE) paper 18163, *Proc. 63rd Sot. Petr. Eng. Tech. Conf*., **1988**, Formation Eval. Res. Geol. Section, 571-585.

[10] V. I. Zarembo and M. K. Fedorov, Density of sodium chloride solutions in the temperature range 25-350°C at pressures up to 1000 kg/cm^2, *J. Appl. Chem. USSR*, **1975**, 48, 1949-1953, (English trans).

[11] R. W. Potter II and D. L. Brown, The volumetric properties of sodium chloride solutions from 0 to 500 C at pressures up to 2000 bars based on a regression of available data in the literature, *U.S. Geol. Surv. Bull*., **1977**, 1421-C.

[12] C. T. Chen, L. S. Chen and F. J. Millero, Speed of sound in NaCl, MgClz, NazS04, and MgS04 aqueous solutions as functions of concentration, temperature, and pressure: *J. Acoust. Sot. Am.*, **1978**, 63, 1795-1800.

[13] F. J. Millero, G. K. Ward and P. V. Chetirkin, Relative sound velocities of sea salts at 25°C: *J. Acoust. Sot. Am.*, **1977**, I 61. 1492-1498.
[14] G. Mavko, T. Mukerji, and J. Dvorkin, The Rock Physics Handbook: Tools for Seismic Analysis in Porous Media, **2003**, New York: Cambridge University Press.
[15] F. Gassmann, Über die elastizität poröser medien, *Vierteljahrsschrift der Naturforschenden Gesellschaft in Zurich*, **1951**, 96, 1–23.

SCIENTIA BRUNEIANA

NOTES TO CONTRIBUTORS

Manuscript Submission and Specifications

Scientia Bruneiana is published twice a year. The deadline for submission of manuscripts is **30th June for the end of year edition** and the **31st December for the May edition**.

Manuscripts should be submitted in Microsoft Office Word (.DOCX) format to the Scientia Bruneiana website, at https://scibru.fos.ubd.edu.bn.

Papers will be refereed prior to acceptance. Authors are welcome to suggest potential international referees.

Articles outlining original research findings as well as mini-review articles are welcomed. There are two special categories: "Brief Communications" and "Research Notes". Contributions to either category should be 300 to 1000 words long (no more than 3 pages in length). The "Research Notes" section is earmarked for summaries of the results and outcomes of projects receiving UBD Science Faculty research grants.

Manuscripts should be written in English (British or American). All manuscripts should be in 12pt Times New Roman, **single-spaced**, **single column** and A4 formatted (2cm margins from the edge).

Title page

The first page should include the title of the article, author's names and addresses of the institutions involved in the work. The paper title is only capitalized on proper nouns and the first letter. Latin, scientific genus and species should be italicized. The authors' affiliations are denoted with a superscripted number and the corresponding author denoted with a * at the end of the author's name. Only the corresponding author's email need to be listed.

Example format of the title page:

First record and conservation value of *Periophthalmus malaccensis* Eggert from Borneo

First Author[1], John H. Smith[2,3], Muhamad Ali Abdullah[2] and Siti Nurul Halimah Hj. Ahmad[1]*

[1]Environmental and Life Sciences, Faculty of Science, Universiti Brunei Darussalam, Jalan Tungku Link, Gadong, BE1410, Brunei Darussalam
[2]Department of Chemical Sciences, Faculty of Science, Universiti Brunei Darussalam, Jalan Tungku Link, Gadong, BE1410, Brunei Darussalam
[3]Department, University, Street Adress, Postcode, Country

**corresponding author email: corresponding.author@ubd.edu.bn*

Abstract Page and Index Terms

The second page of the manuscript should include the abstract (up to 300 words) and index terms (subject heading, or descriptor, in information retrieval, that captures the essence of the topic of a document).

Example format of the abstract and index terms page:

Abstract

The abstract is a self-contained description of the work in one paragraph of up to 300 words. It must include no references or foot notes, but it must describe the key points of the work. This should include

a description of the work that was done and why it was it done. It should include brief conclusions and any significant numerical findings such as derived constants or important parameters.

Index Terms: resolution, spectroscopy, microscopy

Main body of text

For original research articles, the main body of text of the manuscript should include the following appropriately numbered sections: **1. Introduction**, **2. Experimental approach**, **3. Results and Discussions** and **4. Conclusion** followed by **Acknowledgements**, **References** and **Appendices** (if necessary).

Each different numbered section may contain italicised subheadings which are numbered appropriately, e.g. *2.1*, *3.1*, etc.

Review articles will obviously not conform to this format. In the case of other submissions where the above format may be unsuitable, you are advised to contact the editor prior to submitting the article.

Reference to figures, tables and equations

The main body of text should not include figures and/or tables, but should refer to figures and tables. If a certain figure or table was not referred to in the main body of text then it will be considered irrelevant and therefore will not be included in the publication. When referring to a figure or table in the text, the words figure and/or table should be bold and italicized e.g. ***Figure 1*** and ***Table 1***. The words "figure" and "table" should be spelled out in full and not abbreviated. For further instructions on figures and tables (including dimensions, colour schemes and formats), please refer to the figures and tables section (below).

Equations could be displayed in-line or centred by itself, but must be accompanied by a number and individual terms/symbols explained. When When referring to the equation in the text, the word "Equation" should be bold and italicized e.g. ***Equation 1***. The words "Equation" should be spelled out in full and not abbreviated.

Example format of equation:

An example of an equation is shown for ***Equation 1***, Weber Morris intraparticle diffusion:

$$q_t = k_{id} t^{1/2} + C \qquad (1)$$

and Boyd model (***Equation 2***):

$$F = 1 - \frac{6}{\pi^2} exp(-B_t) \qquad (2)$$

where F = q_t / q_e, F is the fraction of solute adsorbed at any time, t and B_t is mathematical function of F.

In-line citation style

The in-line citation should be in IEEE referencing format (numbers with square brackets), generated using a reference manager. Example:

> Even though various studies have shown this [1]–[5], there are others that have contradicted this [6]–[10]. Data was obtained from [11].

Please note that brackets should go **before** punctuation.

References

The reference/bibliographic list should only include references cited in the text and should be listed in the references section in the following format:

> Journal article
> [1] J. H. Surname and J. E. Doe, "Title," *Journal*, Vol., No., Pages, Year. DOI: (number)

Textbook/Chapter of a book
[2] J. H. Surname and J.E. Doe, *Title of Textbook*, Publication House, Year.

Dissertation/Thesis
[3] J.H. Surname, "Title of Thesis," University, Year

Webpages/Online Databases
[4] "Website/Database name/body," Year. Available: http;//www.weburl.com. [Accessed 18-Apr-2017]

These should be generated automatically if a reference manager software has been used. When there are **three or more authors**, just state the name of the first author, e.g. J. H. Surname, et. al. Please include the digital object identifier (DOI) for journal articles.

Figures and Tables

A list of tables, figures and captions should be given at the end of the manuscript after the reference list. These must be appropriately numbered in the order that they appear in the paper. Each table and figure must be adequately discussed and referenced in the text. It is important that you do not include tables and figures in the main body of text of your submitted manuscript.

Sizing

Please keep tables/figures/images/illustrations to have a **maximum width of either 8.4 cm (single column) or 17.5 cm (double column)**, with enough clarity that the images does not appear blurred, skewed or pixelated (unless the pixelation is unavoidable from the raw data collection).

Text

Texts in figures and tables should be 10pt, using either Times New Roman, Arial or Calibri font, with consistent font size and style throughout the manuscript's figures/tables/artwork/images/illustrations. Please ensure that texts do not fall below 8pt size as this will greatly affect readability of said text.

Colour

Colour images are highly encouraged for the on-line issue, however they should be designed such that the information is still obvious in grey-scale too for the print version.

Graphs

Graphs could either be saved as an embedded graph format in DOCX or as an image (JPEG or TIFF). Graphs should have clearly-labelled axes and lines that can be distinguished in both color for on-line and grey-scale for print version. You can use dotted and dashed lines etc, or you can use different data point types when appropriate to discriminate between data sets.

Tables

Tables could either be saved as an embedded table format in DOCX or as an image (JPEG or TIFF), with appropriate captions/titles.

Captions

All figures and tables should be appropriately captioned. The caption should be sufficiently able to explain the figure/table without the reader having to refer to the main text. The words "figure" and/or "table" should be bold. italicized and spelled out fully (not abbreviated), followed by a full stop (also bold and italicized). The rest of the caption should not be bold and italicized (unless it is a scientific genus or species).

Example format for figure/table caption:

> ***Figure 1.*** *Periophthalmus malaccensis* collected in Sungai Bunga, Brunei (UBDM MBu081013mal); a. freshly dead specimen, lateral view; b. live specimen; c. freshly dead specimen, ventral view, detail (scale bars are 10 mm long).

Manuscripts that do not conform to the above instructions will be returned without review.